Coordination of nephrogenesis with branching of the urinary collecting system, the vasculature and the nervous system

Dagmar Iber[a,b,*], **Malte Mederacke**[a,b], **and Roman Vetter**[a,b]
[a]Department of Biosystems Science and Engineering, ETH Zürich, Basel, Switzerland
[b]Swiss Institute of Bioinformatics, Basel, Switzerland
*Corresponding author. e-mail address: dagmar.iber@bsse.ethz.ch

Contents

1. Architecture function of the kidney 2
2. Design principles of epithelial and vascular networks 4
3. Kidney development 5
4. Control of branching morphogenesis 7
   4.1 Signaling networks controlling branching morphogenesis 7
   4.2 Geometry-induced patterning 8
   4.3 Turing mechanism 12
   4.4 Chemotaxis and differential adhesion 16
   4.5 Differential growth and mechanical buckling 18
   4.6 Bud formation and branch outgrowth 21
5. Coordination of nephrogenesis with the formation of the collecting ducts 23
   5.1 Control of nephron numbers 25
6. Coordination of nephrogenesis with vasculature development 26
7. Coordinated development of the nervous system 27
8. Conclusion 28
Acknowledgments 29
References 29

The kidney's primary function is to filter waste from the blood circulation and to regulate electrolyte balance. The kidney relies on highly branched networks to maximize the contact surface area between the vasculature and the filtering units, the nephrons. The nephrons are strategically positioned between the terminal branches of the vasculature and the collecting system. In this review, we discuss the developmental mechanisms that govern their

Current Topics in Developmental Biology
ISSN 0070-2153, https://doi.org/10.1016/bs.ctdb.2024.11.008

coordinated emergence, and explore the design principles underlying the architecture of the epithelial and vascular networks.

1. Architecture & function of the kidney

The kidneys receive up to 20–25 % of cardiac output, amounting to about 1 liter per minute, even though they constitute less than 1 % of body mass (Mohamed and Sequeira-Lopez, 2019). Efficient filtering of those large blood volumes is achieved by maximization of the contact surface area between vasculature and filtering units through highly branched network architectures (Fig. 1A). The filter units, a part of nephrons, are positioned at the interface of the terminal branches of the highly branched trees of the

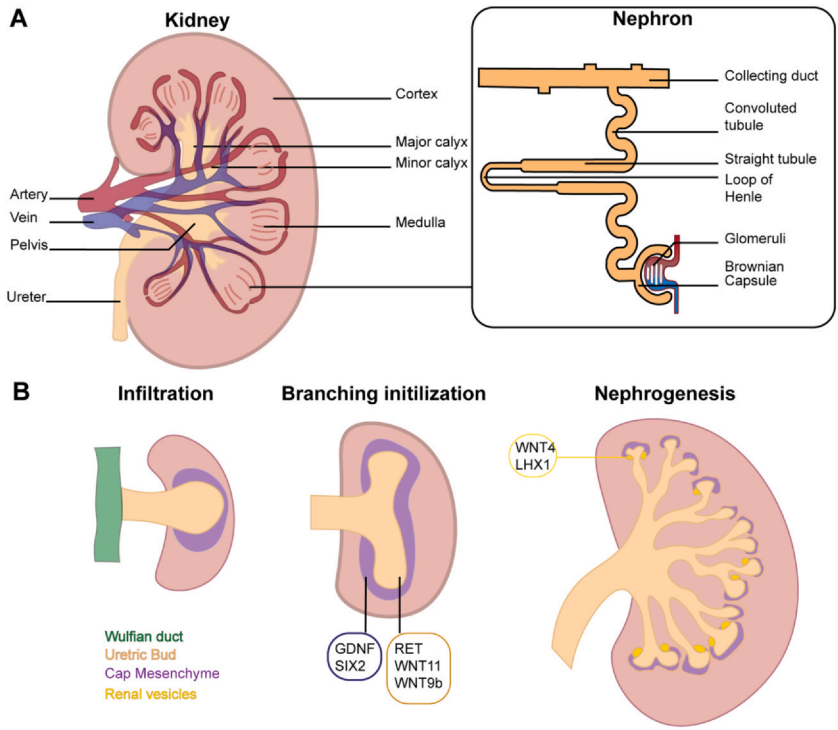

Fig. 1 Development of a functional kidney architecture. (A) The kidney morphology is optimized to fulfill its function. Functional units, the nephrons, are distributed in the kidney medullae and connected to the branched ureter. (B) The kidney develops from the UB, originating from the Wolffian duct and invading the MM. UB branching morphogenesis is coupled to nephrogenesis.

vasculature and the urinary collecting system. Nephron numbers vary widely between individuals, but each human kidney comprises about a million nephrons on average (Mohamed and Sequeira-Lopez, 2019), packed within a bean-shaped anatomy, which measure about 12 cm in length, 6 cm in width, and 4 cm in depth.

Nephrons interface with the vasculature at the glomerulus, a tuft of capillaries lined by endothelial cells and encased by podocytes. Each glomerulus measures approximately 200 μm in diameter in humans (Samuel, Hoy, Douglas-Denton, Hughson, & Bertram, 2007) and is located within a cup-shaped structure, Bowman's capsule (Fig. 1A). The glomerular filtration rate of both kidneys together amounts to about 120 ml/min (Williams, Kenyon, & Adamson, 2010). The filtrate passes through the proximal convoluted tube, followed by Henle's loop and the distal convoluted tube, that reabsorb nutrients and electrolytes, and leaves the nephron via the connecting tubes into the collecting ducts, where water is reabsorbed. Renal blood flow and glomerular filtration rate are regulated by the autonomic nervous system that tightly innervates the renal vasculature (Williams et al., 2010). Stimulation of renal nerves results in vasoconstriction and a decrease in renal blood flow.

In humans, each collecting tubule is about 20–22 mm long and 20–50 μm wide. Hydrostatic pressure aids in moving secretions through these tubules. As the collecting tubes become wider in diameter, the cells increase in height so that the wall becomes thicker (Kumaran and Hanukoglu, 2020). From the narrow collecting ducts, urine flows through the renal papilla of the renal pyramid into a minor calyx, which measures approximately 6.5 mm in diameter (Sobrinho, Sampaio, & Favorito, 2022). Four or five minor calyces merge to form a major calyx, measuring about 9.3 mm in diameter. Each kidney normally has two or three major calyces, which unite to form the renal pelvis, a flattened and funnel-shaped structure with a diameter of about 7–13 mm. Peristaltic contractions propel the urine via the ureter (3 mm in diameter) to the urinary bladder, where it is stored until it is excreted from the body through the urethra.

To supply the large number of nephrons, the vasculature organizes into a branched network. The largest branch, the renal artery, measures about 5 mm in diameter in humans and originates as a lateral branch of the dorsal aorta (Mohamed and Sequeira-Lopez, 2019). The main renal artery enters the kidney at the hilum and usually divides into an anterior and a posterior branch just before entry into the renal parenchyma, and subsequently branches into segmental arteries. Segmental arteries further divide into interlobar arteries, which run between the renal pyramids towards the

cortex. Interlobar arteries arch over the base of the renal pyramids, forming arcuate arteries that run parallel to the renal capsule. Arcuate arteries give rise to interlobular arteries that extend into the cortex, where they supply blood to the nephrons. Interlobular arteries branch into afferent arterioles that supply blood to the glomeruli. Afferent arterioles lead into the glomerular capillaries, where blood filtration occurs. Blood exits the glomerulus via efferent arterioles, which then branch into two distinct networks. Peritubular capillaries surround the proximal and distal tubules, facilitating reabsorption and secretion processes. Vasa recta are specialized capillaries that descend into the medulla, playing a crucial role in the concentration of urine.

In summary, the kidney comprises three distinct branched networks, the epithelial collecting ducts, the vasculature, and the nerves. In the next section, we will present the design principles by which the branched networks are organized to ensure efficient transport and filtering.

2. Design principles of epithelial and vascular networks

In any branching flow system, living or non-living, that is subject to flow resistance minimization within a specified volume, transport between a common inlet (or outlet) and a large number of sinks (or sources) is most efficient if the connecting tubes are organized into a branched dichotomous network whose diameters shrink by a constant factor of $2^{-1/3} = 0.79$ from generation to generation, a relationship known as the Hess-Murray law (Hess, 1914; Murray, 1926b). This fractal relationship has since been confirmed in the bronchial tree and pulmonary capillaries, though only when branch diameters are averaged in each branch generation (Counter, Wang, Farncombe, & Labiris, 2013; Horsfield and Cumming, 1968; Weibel and Gomez, 1962). Individual branches deviate substantially from the common shrinkage factor (Weibel, 1963), but follow Murray's law, as shown for the adult renal arterial network (Nordsletten, Blackett, Bentley, Ritman, & Smith, 2006; Rahmani et al., 2023). According to Murray's law, the radius cubed of the parent branch is equal to the sum of the radii cubed of the daughter branches (Murray, 1926b). Murray's law is equivalent to the Hess-Murray law in case of symmetric branching, but also applies in case of asymmetric branching when the diameters of sister branches are unequal. Networks that organize according to Murray's law are characterized by uniform wall shear stress if the luminal fluid is incompressible and

Newtonian. The fractal architecture could therefore emerge if the epithelial tube diameter were set based on the local shear stress level (Zamir, 1977).

Even though individual branch shapes vary substantially (Weibel, 1963), the length of bronchial tubes is on average about three times larger than their diameter (Nelson, West, & Goldberger, 1990). Assuming constant wall shear stress levels and constant length-to-diameter ratios, the pressure drop is the same across all branches.

Finally, the branch angles have been proposed to minimize the total tube volume necessary to connect source and sink (Bejan, Rocha, & Lorente, 2000; Horsfield and Cumming, 1967; Murray, 1926a; Sciubba, 2016; Uylings, 1977). In case of symmetric branching and $h = 2^{-1/3} = 0.79$, a bifurcating branch angle of 75 degrees would be expected (Horsfield and Cumming, 1967; Murray, 1926a); the reported average angle in the lung is rather close (Horsfield and Cumming, 1967; Phalen, Yeh, Schum, & Raabe, 1978; Thurlbeck and Horsfield, 1980). While fluid flow in the developing lung and kidney is likely laminar, air flow in the human adult lung is turbulent in the first four branch generations and transitions to laminar flow in the fifth generation (O'Connor, Hanley, Mulcahey, Sheets, & Shuey, 2017). The branch angle has been argued to influence the transition from laminar to turbulent flow in that a larger branching angle results in larger and more abrupt changes in momentum and thus promotes turbulence (Rossitti and Lofgren, 1993).

In conclusion, the fractal-like epithelial and vascular networks likely represent an optimal global design, considering all physiological constraints (Mauroy, Filoche, Weibel, & Sapoval, 2004; Wilson, 1967). But what are the local cues that allow cells to organize into a globally optimal architecture? Rather realistic bronchial trees can be created computationally based on nine simple rules (Kitaoka, Takaki, & Suki, 1999). Similarly, rule-based models can recapitulate branching of the ureteric tree (Lefevre et al., 2017). In the following, we will be concerned with the molecular mechanisms from which such rules can emerge and how development of the fractal epithelial, vascular, and nervous networks is coordinated.

3. Kidney development

As a testament to their evolutionary history, mammals successively develop three different kidney structures (Davidson, Lewis, Przepiorski, & Sander, 2019). The pronephros is the earliest, transient kidney structure, but is functional only in lower vertebrates. The second form, the

mesonephros, serves as a temporary kidney in the early human embryo and contributes to the development of the male reproductive system. Finally, the permanent kidney, the metanephros, begins to develop around the fifth week of gestation in humans and around embryonic day (E) 10.5 in mice and will be the focus of this review.

Metanephric kidney development is a complex process that requires the coordinated development of different tissue types. Several excellent reviews provide a detailed introduction, e.g. (Costantini and Kopan, 2010; Little and McMahon, 2012). In the following, we provide a brief overview and then focus on the key principles of developmental self-organization. The pronephros, mesonephros and metanephros all derive from the intermediate mesoderm (IM), a specific region of the embryonic mesoderm that is located between the somites and the lateral plate mesoderm (Davidson et al., 2019). Metanephric kidney development begins with the evagination of an epithelial bud from the caudal portion of the mesonephric (Wolffian) duct, which originates from the anterior IM (Fig. 1B). The ureteric bud (UB) invades the metanephric mesenchyme (MM), a derivative of the posterior IM, in response to GDNF secretion. The expression of *Gdnf* in the MM depends on the Hox paralogs *Hoxa11/Hoxc11/Hoxd11* (Wellik, Hawkes, & Capecchi, 2002), such that the Hox code along the rostral-caudal axis limits kidney development to the hindlimb level (Deschamps and Duboule, 2017). The UB undergoes repeated rounds of branching, forming an epithelial tree that gives rise to the ureter and the collecting duct system, including the renal pelvis, major and minor calyces, and collecting ducts. The MM differentiates into nephron structures, including the renal corpuscle (glomerulus and Bowman's capsule), proximal tubule, loop of Henle, distal tubule, and connecting tubule. Newly formed nephrons connect to the collecting duct system, allowing for the filtration and excretion of waste. Nephrons and the collecting system mature, acquiring the ability to filter blood, reabsorb nutrients, and excrete waste. The surrounding vasculature develops concurrently, ensuring proper blood supply and waste removal. After birth, the kidneys continue to grow and mature, reaching full functionality over the first few years of life.

Throughout kidney development, intricate signaling pathways and gene regulatory networks coordinate the spatial and temporal aspects of organ formation. Additionally, tissue mechanics, fluid dynamics, and geometric constraints play crucial roles in shaping the kidney. In the following sections, we will explore the principles of self-organization that enable the kidney to

develop its complex morphology and functionality. We will begin with the control of ureteric branching morphogenesis, followed by nephrogenesis, and then the formation of the vasculature and nervous system.

4. Control of branching morphogenesis

Much as in the lung, the first rounds of UB branching are highly stereotypic (Blanc et al., 2012; Metzger, Klein, Martin, & Krasnow, 2008; Short, Hodson, & Smyth, 2013; Short et al., 2014), indicating that branching morphogenesis is governed by a deterministic process rather than a random one. Stochastic models, as previously proposed (Hannezo et al., 2017), are thus not appropriate for lung and kidney branching morphogenesis. Candidate mechanisms that lead to the same final repetitive pattern, starting from noisy, spatially uniform initial conditions have been identified, including most prominently Turing and Turing-like mechanisms, differential cell-cell adhesion, chemotaxis, and mechanical buckling via differential growth, as previously reviewed (Iber and Mederacke, 2022; Iber and Menshykau, 2013; Lang, Conrad, & Michos, 2018). In addition, it has been hypothesized that geometric effects might support consecutive branching. We emphasize that a meticulous, data-driven evaluation of these various mechanisms is essential to determine the mechanism governing branch point positioning in the kidney. In the following, we present the mechanisms that have been proposed to guide epithelial branching morphogenesis and discuss the experimental evidence for and against them.

4.1 Signaling networks controlling branching morphogenesis

Genetic experiments have identified glial cell line-derived neurotrophic factor (GDNF), a member of the TGF-beta family, and its receptors RET and GPI-anchored subunit GDNF family receptor alpha-1 (GFRα1) as the key signaling factor guiding branching morphogenesis of the UB (Costantini and Kopan, 2010; Majumdar, Vainio, Kispert, McMahon, & McMahon, 2003; Pichel et al., 1996a, b; Sanchez et al., 1996; Treanor et al., 1996). In their absence, no new branches form, while GDNF-loaded beads induce ectopic branch formation (Hellmich, Kos, Cho, Mahon, & Zimmer, 1996; Menshykau et al., 2019; Moore et al., 1996; Pepicelli, Kispert, Rowitch, & McMahon, 1997; Sanchez et al., 1996; Schuchardt, D'Agati, Larsson-Blomberg, Costantini, & Pachnis, 1994; Tang, Cai, Tsai, Wang, & Dressler, 2002). The GDNF receptors RET and GFRα1 are both

restricted to the surface of the epithelial cells of the UB, while GDNF is secreted by the SIX2-positive nephron progenitor cells (NPCs) in the cap mesenchyme (CM) that surrounds each UB (Hellmich et al., 1996; Moore et al., 1996; Pepicelli et al., 1997; Sanchez et al., 1996).

Much as GDNF/RET/GFRα1 in the kidney, fibroblast growth factor (FGF)10 and its receptor FGFR2b are both necessary and sufficient for the formation of new branches in the developing lung, such that the epithelial tubes only elongate in their absence (Bellusci, Grindley, Emoto, Itoh, & Hogan, 1997; De Moerlooze et al., 2000; Min et al., 1998; Pepicelli, Lewis, & McMahon, 1998; Peters et al., 1994; Sekine et al., 1999). Several other signaling factors modulate lung and kidney branching morphogenesis but are not necessary for branching to proceed. To understand how new branches form, we thus need to understand how GDNF-RET and FGF10-FGFR2b signaling complexes concentrate at the epithelial tips of kidneys and lungs, respectively.

Interestingly, even though FGF10 and GDNF belong to distinct protein families, both FGF10 and GDNF signal through the mitogen-activated protein kinase (MAPK) pathway, a sequence of three protein kinases, MAPKKK, MAPKK, and MAPK, that activate each other via phosphorylation. Activity of the MAPK ERK is completely lost from the UB in RET knockouts (Chi et al., 2009). Phosphorylated ERK concentrates at the epithelial tips, and genetic deletion of the MAPKK *Mek1/2* blocks branching in both the lung and kidney, while the buds continue to elongate (Boucherat, Nadeau, Berube-Simard, Charron, & Jeannotte, 2014; Conrad et al., 2021; Fisher, Michael, Barnett, & Davies, 2001; Ihermann-Hella et al., 2014; Ihermann-Hella et al., 2018; Menshykau et al., 2019). Moreover, both pathways converge on the same downstream target, the ETS transcription factors ETV4/ETV5 (Lu et al., 2009). While not necessary for branching in the kidney (De Moerlooze et al., 2000), FGF10/Fgf2b enhances UB branching (Sims-Lucas et al., 2009), and enhanced FGF signaling in knock-out mice of the antagonist *Sprouty* can rescue $Gdnf^{-/-}$ and $Ret^{-/-}$ mutants, which otherwise fail to develop kidneys (Michos et al., 2010). Together, this suggests important parallels between lung and kidney development and a common regulatory paradigm, despite the differences between the key regulatory proteins.

4.2 Geometry-induced patterning

According to one class of proposed mechanisms, the geometry of the bud results in concentration patterns that drive subsequent branching events.

These have been originally proposed for the developing lung. As FGF10 is secreted from the submesothelial mesenchyme (Bellusci et al., 1997) while its receptor FGFR2b is restricted to the surface of the epithelial bud (De Moerlooze et al., 2000), it has been suggested that bifurcating outgrowth might be the result of geometric effects in that the FGF10 concentration profile splits as the lung bud grows closer to the mesothelium (Fig. 2A) (Bellusci et al., 1997; George and Lubkin, 2018; Hirashima, Iwasa, & Morishita, 2009). However, a splitting of the concentration profile would only occur if the outer surface were impermeable, which is unlikely to be the case as growth factors and inhibitors supplemented to the culture medium affect lung and kidney branching morphogenesis (Iber and Menshykau, 2013; Menshykau, Kraemer, & Iber, 2012; Menshykau et al., 2019).

An alternative mechanism has been proposed based on the steepness of the FGF10 gradient (Clément, Blanc, Mauroy, Sapin, & Douady, 2012). If the FGF10 concentration remained constant at the FGF10-secreting source and the FGF10-degrading epithelial bud, then the steepness of the concentration gradient would depend on the distance between these two boundaries, and a read-out mechanism based on the steepness of the concentration gradient could result in splitting outgrowth (Fig. 2B) (Clément et al., 2012). However, lung branching morphogenesis is still observed when *Fgf10* is expressed uniformly in the mesenchyme (Volckaert et al., 2013). In the kidney, the key growth factor *Gdnf* is expressed throughout the metanephric mesenchyme (Hellmich et al., 1996; Moore et al., 1996; Pepicelli et al., 1997; Sanchez et al., 1996). As such, distance-based mechanisms are unlikely to apply to either organ.

Patterns can also result from uniform secretion of a diffusible factor into an open domain (Nelson, VanDuijn, Inman, Fletcher, & Bissell, 2006). Specifically, if a flat circular disc with open boundaries uniformly secretes a diffusible factor, the highest concentration will form at the center of the domain (Fig. 2C) (Iber and Menshykau, 2013; Menshykau et al., 2012). In a flat 2D tissue with small irregularities, diffusion-limited growth can result in branched outgrowth (Fig. 2D), similar to the branching morphogenesis observed in cultured lung epithelium without mesenchyme (Hartmann and Miura, 2006). Alternatively, diffusion of GDNF from a surrounding mesenchymal source can induce branching in an agent-based model of an epithelial explant (Lambert et al., 2018). Such patterning mechanisms, however, lead to random rather than stereotypic patterning (Iber and Menshykau, 2013).

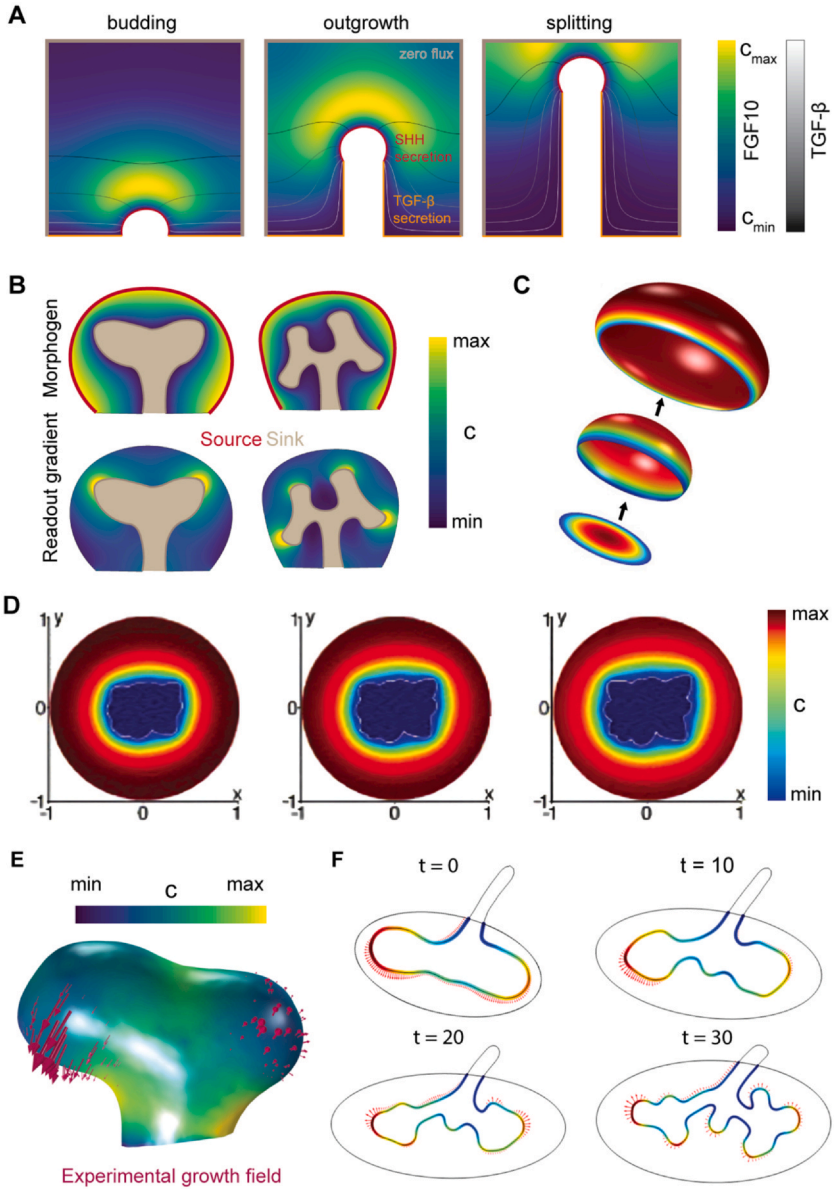

Fig. 2 Geometric effects in branching morphogenesis. (A) Bifurcating outgrowth because of an inhibitor-induced splitting of the FGF10 concentration profile requires an impermeable mesothelial boundary. According to the model by Hirashima et al. (2009), the epithelial bud grows towards the highest concentration of FGF10, which is produced in the mesenchyme and diffuses towards the epithelial surface. SHH, which is secreted from the epithelial tip, activates *Fgf10* expression at low concentration and inhibits it at high concentration. TGF-β, whose concentration levels are indicated by

If the circular disc grows out in 3D, with growth perpendicular to the tissue surface and the growth speed proportional to the concentration of the growth factor, a single bud will emerge from the center (Fig. 2C) (Iber and Menshykau, 2013; Menshykau et al., 2012). However, this mechanism would not support bifurcating outgrowth, as more ligand would be lost from any emerging bud than from the adjacent flat areas, effectively blocking further branching (Menshykau, Blanc, Unal, Sapin, & Iber, 2014). It has been suggested that a growth inhibitor, rather than a growth factor, might be uniformly secreted from the lung bud (Gleghorn, Kwak, Pavlovich, & Nelson, 2012). The loss of this inhibitor from an emerging bud would then support further bud outgrowth. However, a quantitative comparison of the concentration fields and growth patterns in the developing mouse lung does not support this hypothesis (Fig. 2E) (Menshykau et al., 2014). The correlation is slightly better for cultured, flat UBs (Fig. 2F) (Adivarahan, Menshykau, Michos, & Iber, 2013). A better match

isolines following a gray colormap, is secreted from the epithelial stalk and inhibits *Fgf10* expression. Together, this results in a sickle-shaped FGF10 concentration profile around the epithelial tip. If the tip grows close to an impermeable boundary, the sickle shape splits into two domains, located at the two sides of the tip. (B) If the FGF10 concentration was constant at the mesothelium (source) and constant, but lower, at the epithelial surface (sink), then the steepness of the morphogen gradient would be highest at branched tips closest to the mesothelium. This could then support branched outgrowth, in particular if noise was introduced. However, the physiological mechanism that would keep the concentrations constant on the boundary is elusive. (C) If a uniformly produced ligand is secreted from a disc the concentration is highest in the center. If the disc grows perpendicular to its surface with a speed that is proportional to the concentration a bud emerges. However, the bud will not branch. (D) Diffusion-limited growth leads to random branching patterns. (E) Diffusion of a uniformly secreted ligand from the lung bud results in an inhomogeneous concentration profile due to the shape of the bud. The lowest concentrations, however, do not accurately match the observed growth fields (red vectors). The model was simulated on the lung geometry using COMSOL Multiphysics, as previously described (Menshykau et al., 2014). (F) Secretion and diffusion of a uniformly produced growth inhibitor from the UB results in an inhomogeneous concentration profile due to the shape of the UB. Solid colors represent inhibitor concentration (red - low to blue - high). The arrows mark the displacement field, with the length of the arrows indicating the strength of the displacement. *(A) The model from Hirashima et al., 2009 was simulated using COMSOL Multiphysics. (B) The Model from Clément et al., 2012 was simulated using COMSOL Multiphysics. (C) The panel was adapted from (Menshykau et al., 2014). (D) Adapted from (Hartmann and Miura, 2006). (F) The panel was reproduced from (Adivarahan et al., 2013).*

with the observed growth patterns can, however, be achieved using a Turing mechanism (Menshykau et al., 2019), which will be discussed in the next section.

4.3 Turing mechanism

In 1952, Alan Turing described a simple, deterministic mechanism that allows repetitive patterns to emerge from noisy uniform starting conditions (Turing, 1952). The Turing mechanism is based on the interaction of at least two substances that diffuse at different speeds. The wide range of distinct repetitive patterns that can be generated for different parameter sets provides an attractive mechanism to explain the wide range of repetitive patterns that are observed during development. As a result, the Turing patterning mechanism has been proposed to govern a wide range of developmental processes, several of which have since been shown to be controlled differently (Akam, 1989). This highlights the need for careful experimental validation, which has proven difficult for the Turing mechanism.

Several abstract Turing mechanisms have been proposed to explain lung branching morphogenesis (Guo et al., 2014; Meinhardt, 1976; Warburton et al., 2003; Xu, Sun, & Zhao, 2017; Zhu and Yang, 2018), but to test the Turing mechanism experimentally, the identity of the interacting Turing components needs to be defined. Removal of these core Turing factors should eliminate the pattern in the developing tissue, while alterations of their production, turn-over or diffusion rates should affect the distance between patterning elements, the patterning wavelength. The identification of these Turing components has been challenging, not least because of the requirement for different diffusion speeds. Most extracellular ligands have similar diffusion speeds, and small differences mean that the parameter space of the kinetic parameters for which Turing patterns are observed, the Turing parameter space, is small, limiting the evolutionary and developmental robustness of Turing patterning with such ligands.

Decades of sophisticated experiments have revealed the key factors regulating branching morphogenesis in the kidney (Fig. 3A). GDNF, its receptor RET, and their downstream signaling network are the only signaling factors that are both necessary and sufficient for UB branching (Hellmich et al., 1996; Menshykau et al., 2019; Moore et al., 1996; Pepicelli et al., 1997; Sanchez et al., 1996; Tang et al., 2002). GDNF is a dimer (Eigenbrot and Gerber, 1997), and GDNF-RET signaling results in the local up-regulation of the receptor RET (Pepicelli et al., 1997). FGF10 and its receptor FGFR2b, as well as SHH and its receptor PTCH1 form the

same regulatory motif (Ibrahimi et al., 2005; Kadzik et al., 2014; Menshykau et al., 2012; Menshykau et al., 2014). This regulatory motif is consistent with the Schnakenberg kinetics that are well known to result in Turing patterns (Gierer and Meinhardt, 1972; Schnakenberg, 1979). Importantly, since this ligand-receptor-based Turing mechanism is based on the interaction of a ligand with its receptor, only a single extracellular ligand is required (Menshykau and Iber, 2013; Menshykau et al., 2012). The detailed mathematical formulation of the GDNF-RET based Turing mechanism is shown in Fig. 3B. The receptor, R, is produced at rate ρ_R on the epithelial domain, while production of the ligand, L, at rate ρ_L is limited to the surrounding cap mesenchyme. While the production rates are constant in the simplest model formulation, negative feedbacks of ligand-receptor signaling on the constitutive production rates can widen the parameter range for which Turing patterns are obtained, thereby rendering the mechanism more robust to molecular noise and perturbations (Kurics, Menshykau, & Iber, 2014). Ligand binds to the receptors and forms ligand-receptor complexes that result in ligand turn-over and receptor upregulation at rate ν. The necessary difference between the diffusion coefficients emerges naturally. While the ligand diffuses rapidly in the extracellular space, its receptor is membrane bound and thus diffuses slowly on the surface of individual cells. Thus, reported effective diffusion coefficients for extracellular protein ligands, D_L, are in the range 0.1–50 $\mu m^2/s$, while the effective diffusion coefficients for membrane-bound receptors, D_R, are around 0.001–0.1 $\mu m^2/s$ (Menshykau and Iber, 2013). Large differences, i.e. $D_L/D_R >> 1$, result in large Turing parameter spaces, which are further increased by the restriction of receptors to single cells (Kurics et al., 2014). The smaller the cells, the larger the Turing parameter space (Kurics et al., 2014). Given the wide parameter ranges, for which Turing patterns emerge for this ligand-receptor-based motif, its evolutionary emergence is highly plausible. The patterning process is stable on growing domains and supports the emergence of buds as well as bifurcating outgrowth (Fig. 3C).

One well-known limitation of Turing mechanisms is its pattern sensitivity to the noisy initial conditions (Arcuri and Murray, 1986). Thus, the same parameter set can yield very different patterns for slightly different noisy initial conditions (Adivarahan et al., 2013; Menshykau and Iber, 2013; Menshykau et al., 2014). The pattern of the ligand-receptor complex predicted by the ligand-receptor-based Turing mechanism is, however, quantitatively consistent with the observed growth fields in embryonic

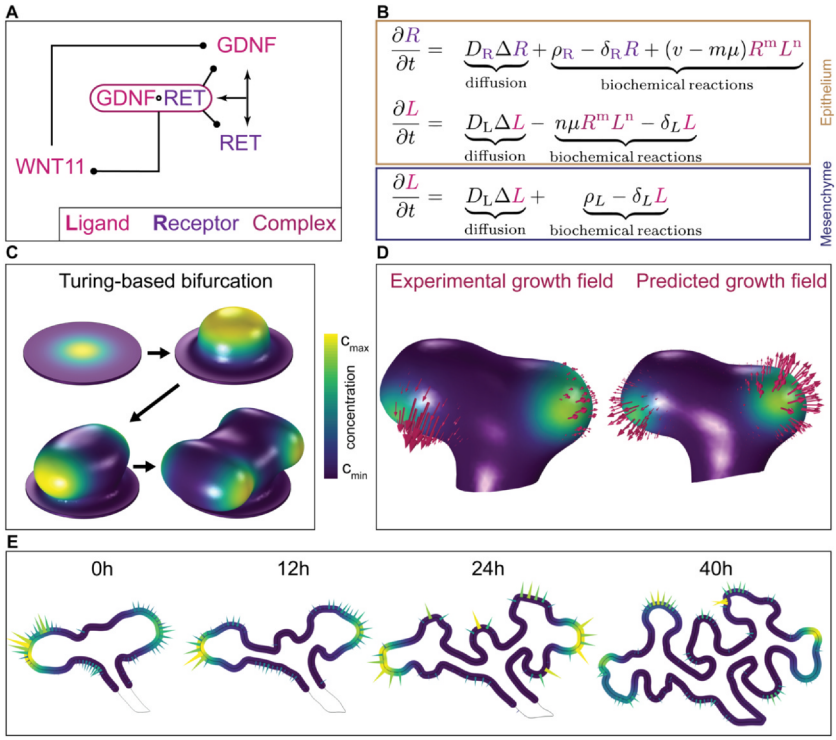

Fig. 3 Turing patterns guiding branching morphogenesis. (A) Regulatory network driving branching of the UB. Mesenchymal, extracellular GDNF diffuses to the UB and binds to its epithelial membrane-bound receptor RET. The GDNF-RET signaling complex upregulates expression of *Ret* and induces secretion of extracellular WNT11, which enhances *Gdnf* expression in the MM. (B) Mathematical representation of the core regulatory network of receptor RET (R) and ligand GDNF (L) in panel A. Production at rate ρ_R, constitutive decay (δ_R) and diffusion (D_R) of the receptor are restricted to the epithelium, while production (ρ_L) of the ligand is restricted to the mesenchyme. The ligand can diffuse in the entire domain (D_L). Accordingly, ligand-receptor complexes can form on the epithelial membrane and result in receptor upregulation at rate v, and removal of receptor and ligand at rate μ. m and n are the stoichiometric factors of RET and its dimeric ligand GDNF. Ligand decays everywhere at a small constitutive rate δ_L. Separation of the expression domains for ligand (MM) and receptor (UB) into two separate domains leads to robust patterning via the ligand-receptor-based Turing mechanism. (C) The ligand-receptor-based Turing mechanism can result in robust bifurcations. Domains grow in normal direction at speeds relative to the strength of ligand-receptor signaling, R^2L. (D, E) The patterns of the ligand-receptor complex (colormap) match the experimentally determined growth fields (arrows) in the developing lung (static) (D) and kidney (organ explant culture) (E). *(A) Adapted from (Menshykau et al., 2014). (B) Adapted from (Menshykau et al., 2014; Menshykau et al., 2019).*

lungs (Fig. 3D) and cultured UBs (Fig. 3E) without any such sensitivity to the noisy initial conditions (Menshykau et al., 2014; Menshykau et al., 2019). The reason for the robustness is the separation of the expression domains of ligand and receptor: the expression of the ligand is restricted to the mesenchyme, while its receptor is restricted to the epithelial surface (Adivarahan et al., 2013; Menshykau et al., 2014). The geometry-induced pre-pattern biases the Turing mechanism to a particular pattern for a given parameter set (Menshykau et al., 2014). Consistent with the prediction of the Turing mechanism (Adivarahan et al., 2013; Menshykau et al., 2014), the stereotypic nature of the branching pattern is lost when the ligand GDNF is ectopically expressed in the UB (Shakya et al., 2005). Similarly, if UBs are cultured in Matrigel with GDNF, the branching pattern is random (Conrad et al., 2021).

The Turing mechanism correctly predicts the patterning changes observed in all relevant mutants (Lawson and Flegg, 2016; Menshykau and Iber, 2013; Menshykau et al., 2019). Removal of GDNF or RET prevents bud formation, while removal of Sprouty, an inhibitor of GDNF signaling, results in a smaller distance between buds in the simulations, and the emergence of multiple kidneys in the embryo (Menshykau and Iber, 2013). The model further predicts slightly reduced branching in mice heterozygous for the Ret receptor gene ($Ret^{+/-}$). According to experimental studies, branching is either normal or slightly reduced in $Ret^{+/-}$ mutants (Majumdar et al., 2003). Similarly, in the lung, the Turing mechanism recapitulates all observed perturbations (Celliere, Menshykau, & Iber, 2012), including even counterintuitive mutant phenotypes such as the abrupt increase in the spacing between buds as the *Fgf10* expression levels fall below a threshold in a sequence of *Fgf10* hypomorphic mutants (Mailleux et al., 2005; Menshykau et al., 2012) and normal lung branching morphogenesis when *Fgf10* is expressed uniformly in the mesenchyme (Menshykau et al., 2014; Volckaert et al., 2013). Strikingly, FGF7, which binds to the same receptor as FGF10, but blocks lung branching morphogenesis, has been found to trigger FGFR2b removal, while the receptor returns to the membrane after FGF10-triggered endocytosis (Francavilla et al., 2013). FGF7 thus likely interferes with the upregulation of FGFR2b on the cell membrane that is required for the Turing mechanism.

The core GDNF-RET circuit interacts with WNT11 in a positive feedback loop in the form that GDNF-RET induces WNT11 secretion from the urothelium, while WNT11 enhances GDNF secretion from the MM (Majumdar et al., 2003). The model predicts and experiments confirm

that this positive feedback enables a closer packing of the ureteric tips because the positive feedback replenishes GDNF ligand in the metanephric mesenchyme between the closely packed tips, and thereby enables their closer apposition (Majumdar et al., 2003; Menshykau et al., 2019). The average branching angle in the kidney ranges from 90 to 100 (Mederacke, Conrad, Doumpas, Vetter, & Iber, 2023; Short et al., 2014), resulting in branches growing towards each other after two rounds of branching, such that the tips compete for ligands (Menshykau et al., 2019). Closer packing is also observed upon interference with BMP7 signaling via mutations in *Bmp7* or its antagonist *Gremlin* (Davies, Hohenstein, Chang, & Berry, 2014), likely because of their impact on the GDNF-WNT11 feedback (Michos et al., 2007).

In summary, the Turing mechanism based on the GDNF-RET interaction is qualitatively and quantitatively consistent with data from embryonic kidneys, and the Turing pattern based on the FGF10-FGFR2b interaction matches the wide range of genetic results in the mouse lung.

4.4 Chemotaxis and differential adhesion

Strikingly, despite tight cell-cell adhesion, cells in the UB sort according to RET activity (Riccio, Cebrian, Zong, Hippenmeyer, & Costantini, 2016; Shakya et al., 2005). Cells that fail to express *Ret* become excluded from the ureteric tips and accumulate in the stalk (Chi et al., 2009), while cells, which are genetically forced to maintain *Ret* expression, show the opposite tip-seeking behavior (Packard, Klein, & Costantini, 2021). This tip-seeking behavior depends on GDNF from the mesenchyme (Packard et al., 2021). GDNF has been proposed to act as a chemoattractant for *Ret*-expressing epithelial cells (Tang, Worley, Sanicola, & Dressler, 1998; Tang et al., 2002). Activation of the RET pathway in the MDCK renal epithelial cell line results in increased cell motility, dissociation of cell adhesion, and the migration towards a localized source of GDNF (Tang et al., 1998; Tang et al., 2002). Cellular responses to RET activation include the formation of lamellipodia, filopodia, and reorganization of the actin cytoskeleton. In conclusion, the restriction of *Ret* expression to the tips of the UBs is not only due to the positive signaling feedback of GDNF-RET signaling complexes on *Ret* expression, but also reflects active cell movement in the epithelium in response to GDNF. This opens up the possibility that, in addition to chemical reaction-diffusion, cell motility and interactions play an important role in pattern formation, as previously proposed in the context of skin patterning in zebrafish (Watanabe and Kondo, 2015).

Experiments with mammary epithelial cells embedded in a 3D type I collagen gel showed that highly motile cells (with high MMP14 expression) sorted into end regions, while less motile cells (with low MMP14 expression) were found in the trunk regions (Mori, Gjorevski, Inman, Bissell, & Nelson, 2009).

Chemotaxis and differential cell adhesion can yield rich patterns also without such boundary effects (Fig. 4) (Armstrong, Painter, & Sherratt, 2006; Carrillo, Murakawa, Sato, Togashi, & Trush, 2019; Murray, 1993). The underlying mathematical principle is similar to the one that leads to Turing patterns (Armstrong et al., 2006; Murray, 1993), but the biological implementation would be very different. A quantitative evaluation of this

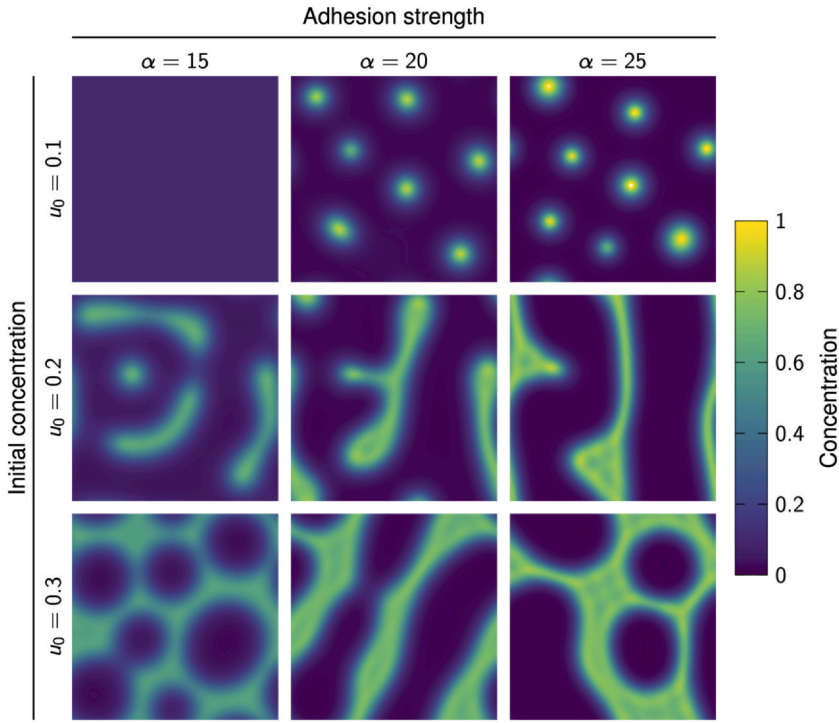

Fig. 4 Patterning by differential adhesion. Transient patterns obtained from numerical continuum simulations of differential cell adhesion. The Armstrong model (Armstrong et al., 2006) was solved in a periodic square domain with an edge length of ten times the adhesion sensing radius, for different dimensionless adhesion strengths a and relative initial cell concentrations u_0. Images show snapshots taken at equal dimensionless timepoints, = 10. Simulations carried out in COMSOL Multiphysics by Chengyou Yu.

candidate mechanism with data from kidney development would therefore be important. Chemotaxis and differential adhesion have so far mainly been modeled with discrete agent-based models and continuum models based on partial differential equations (Armstrong et al., 2006; Hillen and Painter, 2009; Murray, 1993; Pleyer and Fleck, 2023). Recently developed simulation frameworks now make it possible to efficiently simulate also large 3D epithelial tissues at high geometric resolution (Runser, Vetter, & Iber, 2024). This will allow for a more realistic test whether the mechanism can apply in an epithelial tube of tightly adhering, polarized cells.

Alternatively, the observed sorting based on RET activity could act in the context of a Turing mechanism that restricts RET activation to the tips. Cell sorting may be important to achieve uniform activation at the tips, given that the ligand-receptor-based Turing mechanism results in salt-and-pepper activation patterns on a cellular domain rather than uniform activation (Kurics et al., 2014). Detailed quantitative measurements in combination with computational modeling will be needed to distinguish between a patterning mechanism based on chemotaxis, differential adhesion, or Turing kinetics.

4.5 Differential growth and mechanical buckling

If tightly attached tissue layers expand at different rates, a buckling instability can cause the tissue to fold in a repetitive pattern. The developing intestine serves as a prominent example (Savin et al., 2011). The distance between folds, known as the patterning wavelength, depends on the material properties of the two tissue layers. In the simplest case of two incompressible, linearly elastic tissue layers with Young's moduli E, the wavelength λ is given by (Biot, 1957)

$$\lambda = 2\pi h \sqrt[3]{\frac{E_1}{3E_2}}$$

where h is the thickness of the thinner and stiffer tissue layer (subscript 1) attached to a softer and considerably thicker layer (subscript 2) (Fig. 5A). Note that for periodic geometries such as tubes with circumference C, the wavelength approximates the above relationship but is rounded to integer fractions of the periodicity: $\lambda = C/n$, where n is the number of undulations (Fig. 5B-D). However, care must be exercised in the attribution of causation when mechanical patterns are observed, as it can be unclear whether tissue folds or wrinkles are indeed causally driven by such a growth-induced mechanical instability or whether they just emerge at the right

length scale due to the necessarily compatible mechanical properties of the tissue to produce a spatial pattern that may actually be caused through a different mechanism originally. Of note, differential growth on curved geometries often yields folds and stripes rather than buds (Tan, Hu, Song, Chu, & Wu, 2020), and the pattern mechanically tends to be non-local unless confined through a separate prepatterning mechanism. On a tube of a uniform material, for example, buckling instabilities produce primary undulations that span the entire circumference (Zhao, Cao, Feng, & Ma, 2014). To localize patterns to bud formation sites, the tissue would need to be non-uniform to begin with, grow non-uniformly, or respond highly non-linearly to small shape perturbations. It remains to be seen whether differential growth in combination with additional effects could yield the observed morphologies.

Considering that branching morphogenesis is still observed in the absence of the mesenchyme, as long as the growth factor FGF10 or GDNF are provided in the culture medium of lung and kidney epithelial explants, respectively (Bellusci et al., 1997; Conrad et al., 2021; Hartmann and Miura, 2006; Nogawa and Ito, 1995; Ohtsuka, Urase, Momoi, & Nogawa, 2001; Park, Miranda, Lebeche, Hashimoto, & Cardoso, 1998; Qiao, Sakurai, & Nigam, 1999; Varner, Gleghorn, Miller, Radisky, & Nelson, 2015), differential growth between epithelium and mesenchyme seems not to be necessary for bud formation. Rather than serving a structural role, the reciprocal interaction between the UB and the surrounding metanephric mesenchyme appears to be necessary for chemical signaling, in particular between FGF10/GDNF in the mesenchyme and their respective receptors on the epithelium.

Bud formation could still be the result of differential growth between the epithelium and the extracellular matrix (ECM) that covers the basal surface of the UB, as proposed for the airway epithelium (Varner et al., 2015). However, buckling will occur only if the thin, stiff ECM expands more than the thick, soft epithelium (Fig. 5B-D). If the epithelium expands more than the ECM, then the ECM will only be stretched, but remains smooth (Fig. 5E). Considering that growth is driven by the epithelial cells, stronger growth of the ECM is rather unlikely. Inconsistently with such a mechanism, weak inhibition of matrix metalloproteases (MMP), which normally degrade and thin ECM at the lung tips, enhances lung growth and branching (Conrad et al., 2021; Gill, Pape, Khokha, Watson, & Leco, 2003; Gill, Pape, & Leco, 2006). If ECM expansion relative to the epithelium was to drive buckling, then a thinning of the ECM should result in

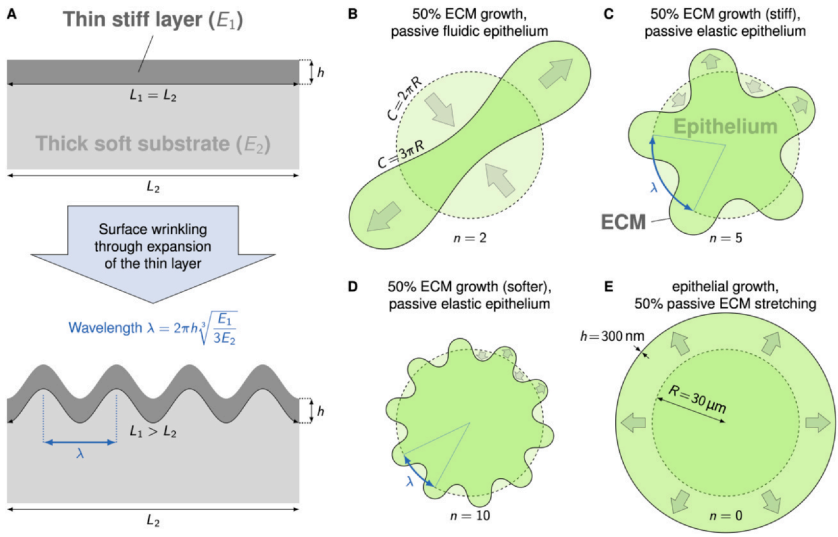

Fig. 5 Regular mechanical patterning with differential growth. (A) Schematic of buckling due to differential growth between a thin layer on a soft elastic substrate. *h* is the thickness of the thinner and stiffer tissue layer (subscript 1) attached to a softer and considerably thicker layer (subscript 2). Given the stiffness difference between ECM (Young's modulus $E_1 \approx 120$ kPa) and epithelium ($E_2 \approx 100$–1000 Pa), the observed patterning wavelength $\lambda = 100$–150 μm can, in principle, be obtained with the thin ECM ($h < 1$ μm) and a much thicker (30–50 μm) epithelium (Gomez et al., 2021). (B–E) Mechanical equilibrium solutions of a circular cross section of an epithelium (green) surrounded by an ECM layer (black), obtained numerically as detailed in (Vetter, 2015). The luminal space is tiny in early stages of lung and kidney development (Gomez et al., 2021) and is neglected here. Initial configurations are shown as dashed shapes, arrows indicate the deformation. The ECM is grown by 50 % in circumference with the epithelium deforming passively without expanding (B–D), or the epithelium is grown and stretches the ECM passively (E). In B, the epithelium is represented as an incompressible fluid, whereas in C and D, it is an elastic, incompressible, geometrically nonlinear Winkler foundation analogous to (Sultan and Boudaoud, 2008). The ECM is modeled as an elastic beam without spontaneous curvature. The number of buds/wrinkles is indicated as *n*. No buds emerge if the epithelium grows more than the ECM (E).

more buds rather than inhibition of branching. Strong MMP inhibition impairs lung bud outgrowth altogether (Conrad et al., 2021; Gill et al., 2003; Gill et al., 2006) and is thus not informative. Also, the mechanism by which FGF10 and GDNF drive branching morphogenesis would require further investigation. As branches still elongate in the absence of FGF10 and GDNF signaling (Abler, Mansour, & Sun, 2009; Ihermann-Hella et al., 2014; Ihermann-Hella et al., 2018), GDNF and FGF10 would have to exert their necessary role in branching by affecting the ECM. The ECM is

thinner at the lung tips (Gill et al., 2003; Mollard and Dziadek, 1998; Moore et al., 2005; Rutledge, Parvez, Short, Smyth, & McMahon, 2019). While a thinner ECM would be consistent with more branching, a mechanism other than differential growth would first need to break the symmetry and cause the localized ECM thinning.

A chemical Turing mechanism could instead explain the observed branching behavior of lung and kidney epithelial explants (Adivarahan et al., 2013), and patterning via the Turing mechanism would be expected to be affected by changes in the ECM as modulation of the binding to heparan sulfates affects FGF diffusivity (Makarenkova et al., 2009), which in turn determines the wavelength of the pattern. Moreover, heparin has been found to affect signaling of the GDNF-RET complex (Parkash et al., 2008). In conclusion, the ligand-receptor-based Turing mechanism is consistent with all reported data of lung and kidney development.

4.6 Bud formation and branch outgrowth

To form a bud, cell shapes have to change in that the apical cell diameter has to shrink, while the basal diameter has to increase, and the apical-basal axis has to lengthen to maintain a constant cell volume (Kadzik et al., 2014). While differential growth would directly result in bud formation, the other mechanisms discussed above only mark points of branch formation, and buds must subsequently form via active localized cell deformation in response to localized GDNF/RET/ERK or FGF10/FGFR2b/ERK signaling. There is indeed ample evidence that active cell shape changes are necessary for bud formation (Kadzik et al., 2014; Kim, Varner, & Nelson, 2013; Moore et al., 2005). Bud formation has been suggested to be driven by apical constriction (Fumoto, Takigawa-Imamura, Sumiyama, Kaneiwa, & Kikuchi, 2017; Kim et al., 2013; Martin and Goldstein, 2014). However, given the pseudostratified nature of the lung epithelium (Gomez, Dumond, Hodel, Vetter, & Iber, 2021), it is unclear how apical constriction would result in shape changes along the entire apical-basal axis. The Wnt/Fzd2 pathway has been shown to promote cell lengthening via the RhoA pathway (Kadzik et al., 2014), which is also a downstream target of ERK signaling (Iber, 2021). Drugs that inhibit the downstream RhoA target, ROCK, or myosin light chain kinase or myosin ATPase, interfere with myosin light chain (MLC) phosphorylation and reduce lung branching morphogenesis (Moore et al., 2005). Cytotoxic necrotizing factor-1 (CNF-1), a general Rho activator, accelerates epithelial branch formation in cultured embryonic lung

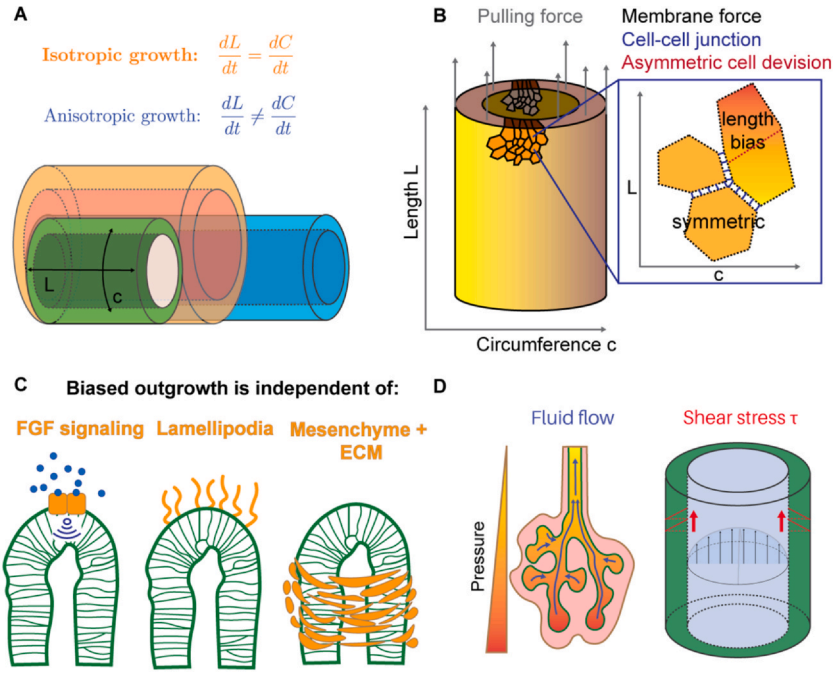

Fig. 6 Biased branch outgrowth. (A) Lung buds preferentially elongate in early lung development. (B) Cells are elongated in direction of outgrowth and divide preferentially perpendicular to their longest axis if the axis ratio exceeds 1.5. (C) Biased growth is the result of neither localized FGF10 signaling, ECM thinning at the tips, active cell migration via lamellipodia, nor active pulling by the mesenchyme. (D) The fluid velocity inside the tubes in early stages of lung development is high enough that the resulting shear stress on the epithelial walls can likely be sensed by cilia.

rudiments (Moore, Huang, Kong, Sunday, & Ingber, 2002; Moore et al., 2005). Cytochalasin D, a drug that disrupts actin microfilament integrity, almost completely inhibits lung branching (Moore et al., 2005).

Once the bud has formed, it must grow out into a branch. Lung buds have been shown to preferentially elongate in early lung development (Fig. 6A) (Conrad et al., 2021; Tang, Marshall, McMahon, Metzger, & Martin, 2011; Tang et al., 2018). Preferential elongation is accompanied by biased cell division in direction of outgrowth (Fig. 6B). The planar cell polarity pathway (PCP) can, in principle regulate mitotic spindle angle distribution (Ciruna, Jenny, Lee, Mlodzik, & Schier, 2006; Gong, Mo, & Fraser, 2004; Saburi et al., 2008), but there is no indication that the PCP pathway regulates spindle orientation in the lung epithelium (Paramore, Trenado-Yuste, Sharan, Nelson, & Devenport, 2024; Tang et al., 2011).

According to Hertwig's rule, cells divide perpendicular to their longest axis (Hertwig, 1884). As long as the apical cell aspect ratio exceeds 1.5, cells in the lung buds indeed divide perpendicular to their longest axis (Tang et al., 2018). Computational modeling shows that this bias in cell shape and cell division is only achieved if biased growth is the result of a pulling rather than a constricting force (Conrad et al., 2021; Stopka, Kokic, & Iber, 2019). Experiments further show that biased growth is the result of neither localized FGF10 signaling, ECM thinning at the tips, active cell migration via lamellipodia, nor active pulling by the mesenchyme (Fig. 6C) (Conrad et al., 2021). Rather, the velocity of the fluid flow inside the tubes in those early stages of lung development is high enough that the resulting shear stress on the epithelial walls can likely be sensed by cilia (Fig. 6D) (Conrad et al., 2021). Mutations that interfere or block cilia maturation reduce or prevent biased outgrowth, respectively (Tang et al., 2011; Zeng et al., 2024). Whether a similar mechanism operates in the UB remains to be seen, but fluid flow has been reported once the nascent nephrons have connected to the UB.

While the average dihedral angle is similar in the developing kidney and lung (60–70 degrees), the average bifurcation angle (90–100 degrees) is much larger in the developing kidney (Mederacke et al., 2023; Short et al., 2013; Short et al., 2014). The branch lengths and angles found in developing kidneys place endpoints in a single layer at a uniform distance from the center of the organ, while those found in the later stages of lung development result in a 3D space-filling pattern (Yu et al., 2019). Unlike in the lung, tips in the developing kidney are tightly packed on the surface (Prahl, Viola, Liu, & Hughes, 2021). The branching angle depends on the organ-specific mesenchyme (Blanc et al., 2012; Lin et al., 2003; Sakakura, Nishizuka, & Dawe, 1976), but the mechanism by which the organ-specific branching angles are set has remained elusive.

5. Coordination of nephrogenesis with the formation of the collecting ducts

To ensure efficient drainage, nephrogenesis and branching morphogenesis must be tightly coordinated. Nephrons are formed by NPCs from the cap mesenchyme that condense in the branch corners and undergo a mesenchymal-epithelial transition (MET) to form pretubular aggregates (PTA) that further mature into renal vesicles (RVs), which grow

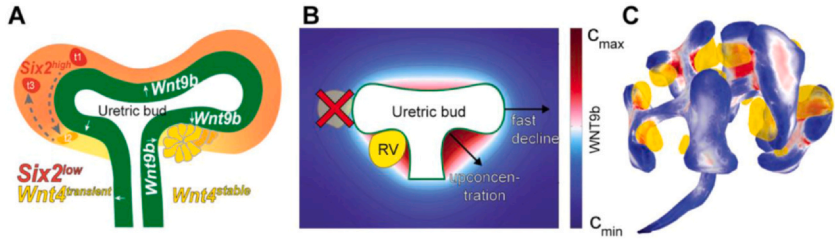

Fig. 7 Coordination of nephrogenesis and branching morphogenesis. (A) The key regulator of nephrogenesis, WNT9b, is uniformly secreted from the UB epithelium (green). While SIX2 positive nephron progenitor cells (orange) are uniformly covering the entire epithelium and are actively migrating, differentiation into pretubular aggregates that subsequently mature into renal vesicles (yellow) only happens in branch corners. (B) For a sufficiently small branch angle and high curvature uniformly secreted WNT9b accumulates in the branch corners of UBs. The concentration increases on concave surfaces, while convex areas lead to a faster decline. The required curvature depends on the characteristic length of the gradient. (C) Simulating secretion and diffusion of WNT9b on E12.5 UB geometries confirms that the highest predicted WNT9b concentrations coincide with the position of pretubular aggregates and renal vesicles. *A-C are adapted from (Mederacke et al., 2023).*

out into S-shaped bodies, which finally elongate and mature into nephrons (Little, 2015; Oxburgh, 2018; Perl, Schuh, & Kopan, 2022).

Reciprocal signaling between UB and MM ensures that a single nephron emerges in each branch corner and fuses to the ureteric tree (Fig. 7A). Genetic experiments have identified WNT9b as the most upstream inducer of nephrogenesis (Carroll, Park, Hayashi, Majumdar, & McMahon, 2005). WNT9b is secreted from the UB and induces expression of *Wnt4* in the adjacent MM. WNT4 suppresses expression of *Six2*, a transcription factor that supports its own expression and that is necessary for the renewal of NPCs (Self et al., 2006). Loss of SIX2 results in the differentiation of NPCs into epithelial cells that condense into PTAs, which reduces the GDNF-secreting pool of cap mesenchyme cells, which in turn affects branching morphogenesis of the ureter.

There has been a long quest for molecular factors that restrict nephrogenesis to the branch corners as WNT9 is secreted largely uniformly from the UB, and the SIX2-positive cap mesenchyme covers most of the ureteric tip and all SIX2-positive NPCs are, in principle, responsive to WNT signals. However, no further gene was found that would explain the positioning of nephrogenesis. While it has been argued that signals from the stroma (potentially mediated by the transcription factor FOXD1) might limit nephrogenesis to the branch corners (Oxburgh, 2018), nephrogenesis

is still restricted to the branch corners when explants of the ureteric bud are co-cultured with scrambled MM (Mederacke et al., 2023). Computational simulations based on 3D geometries of the developing kidney have recently demonstrated that WNT9b, when uniformly secreted from the UB surface, concentrates in the branch corners due to geometric effects (Fig. 7B), without a requirement for further regulatory factors (Mederacke et al., 2023). As the UB acts as a diffusion barrier for the secreted WNT9b, WNT9b becomes locally concentrated in the branch corners even though WNT9b is largely uniformly secreted (Fig. 7C). The WNT9b concentration is highest, the smaller the branching angle and the higher the curvature. The angles between parent and daughter branch are indeed the smallest that permit continued branching, and the curvature is the highest that can accommodate the RV size (Mederacke et al., 2023; Short et al., 2014). For a plausible WNT9b gradient length in the range 20–40 μm, a 2-fold increase in the WNT9b concentration can be expected in the branch corners (Mederacke et al., 2023). NPCs sensitively respond to a 2-fold difference in the WNT9b concentration and β-catenin activity (Mederacke et al., 2023). A previous study argued against geometric effects because NPCs differentiate when placed adjacent to a WNT1-secreting tissue piece, no matter whether the tissue border is concave or convex (Ramalingam et al., 2018). However, image-based modeling based on the published geometry of the used tissue demonstrates that the lack of an observed curvature effect can be accounted for by the too low overall curvature of the tissue used in the experiment (Mederacke et al., 2023).

Importantly, NPCs are highly motile, and *Wnt4*-expressing NPCs that migrate out of the branch corner can return to the progenitor pool (Combes, Lefevre, Wilson, Hamilton, & Little, 2016; Lawlor et al., 2019; Lindstrom et al., 2018). This further ensures that differentiation remains restricted to the corner region. WNT4 and FGF8 engage in positive feedback, enhancing each other's expression (Perantoni et al., 2005). FGF8 increases the speed and motility of NPCs, thereby facilitating the emergence of cell condensations (Sharma et al., 2022). Cell-based computational models can be employed to define the range of spatio-temporal patterns of motility and cell-cell adhesion that can drive the emergence of cell condensations (Sharma et al., 2022; Tikka et al., 2022).

5.1 Control of nephron numbers

The total number of nephrons varies between individuals over at least one order of magnitude, with consequences for the functionality of the kidney

(Bertram, Douglas-Denton, Diouf, Hughson, & Hoy, 2011; Bueters, van de Kar, & Schreuder, 2013; Hoy, Hughson, Bertram, Douglas-Denton, & Amann, 2005; Keller, Zimmer, Mall, Ritz, & Amann, 2003; Lambert et al., 2018). Several genetic alterations have been identified that affect kidney size, including *PAX2* haploinsufficiency, which causes renal-coloboma syndrome, or hypomorphic variants of the *RET* gene (Dziarmaga et al., 2003; Zhang et al., 2008). The total nephron number depends on the continued expansion of the metanephric mesenchyme, which secretes the growth factor GDNF that is required for the continued branching of the UB. The balance between the proliferation of the SIX2-positive NPCs and the epithelial cells in the UBs likely determines the final number of nephrons, as has also been explored in mathematical models (Zubkov et al., 2015). Termination of tip branching within the developing kidney has been accounted for by stochastic exhaustion in response to NPC differentiation during nephrogenesis (Hannezo et al., 2017). However, experiments have since shown that nephrogenesis neither impacts the branching program nor cell proliferation in either tip or progenitor cell niches (Short et al., 2018), thus rejecting a nephrogenesis-based termination mechanism.

6. Coordination of nephrogenesis with vasculature development

Renal vasculature development must be highly coordinated with nephrogenesis to build a functional kidney. Each nephron must be vascularized by capillaries that organize into a branched network and are connected to the blood circulation. The renal vasculature develops both de novo by vasculogenesis and via angiogenic growth of arteries that connect to the aorta (McMahon, 2016; Munro and Davies, 2018). Vascular cords first surround the metanephros at embryonic day (E) 10.5 (Daniel et al., 2018; Munro and Davies, 2018), and form a CD31-positive vascular ring around the stalk of the UB by E11.25 (Munro et al., 2017). By E11.5, endothelial vessels are observed in the MM, and by E12.5, the entire metanephros is vascularized (Munro and Davies, 2018). Continued growth, remodeling and maturation of the endothelial network leads to the establishment of an arterial tree by E13.5 that forms a predictable pattern, pointing to its stereotypic development (Daniel et al., 2018; Honeycutt et al., 2023). The stroma is required for development of the renal vasculature and secretes, among others, the angiogenic factor laminin-like

protein netrin 1 (Ntn1), which is required for the emergence of arterial vascular smooth muscle cells (vSMC), and without which arterial branching is severely reduced from E15.5 (Luo, Gu, Chaney, Carroll, & Cleaver, 2023). The renal arterioles are first evident at E15 in mouse embryos (Sequeira Lopez and Gomez, 2011). From E13.5 and throughout embryonic development, polygonal endothelial networks, or endothelial plexuses, surround UB ampullae in the nephrogenic zone. As nephrons form, the S-shaped body is infiltrated by endothelial cells to generate a primitive vascular tuft within the cup-shaped glomerular precursor region. This process is heavily influenced by signals from podocytes and other glomerular cells, including VEGF. VEGF also controls the development of the pulmonary capillary network. In the lung, mesenchymal *Vegfa* expression is controlled by Sonic Hedgehog (SHH) and FGF9 (White, Lavine, & Ornitz, 2007), and thus linked to the development of the bronchial tree (Celliere et al., 2012). Whether a similar coordination exists also in the kidney remains to be seen.

As the renal arterial network develops, blood flow begins, imposing hemodynamic forces that influence further vascular maturation and nephron differentiation. As nephron segments become functional, their activities influence blood flow and pressure, creating a dynamic feedback loop that further refines vascular and nephron development.

The vessel architecture is the result of extensive pruning during development with considerable variability between individuals that needs to be taken into consideration in kidney transplantations (Arevalo Perez et al., 2013). These variations may be explained by the ascending course of the kidney in the retroperitoneal space, from the original embryological site of formation (pelvis) to the final destination (lumbar area). During this course, the kidneys are supplied by consecutive branches of the iliac vessels and the aorta. Usually, the lower branches become atrophic and vanish while new, higher ones supply the kidney during its ascent. Accessory supernumerary arteries are common (in about 25% of humans). If a supernumerary artery does not enter the kidney through the hilum, it is called aberrant.

7. Coordinated development of the nervous system

Renal innervation begins at E13.5 (Honeycutt et al., 2023; N'Guetta et al., 2024b; Tarnick, Elhendawi, Holland, Chang, & Davies, 2023).

Axonal projections tightly associate and track with existing renal vasculature, forming tight neurovascular bundles (Honeycutt et al., 2023; Tarnick et al., 2023). As the vascular tree branches and becomes more complex, the nerves also branch and refine their pattern, closely mirroring the vasculature. This close association is maintained as the vessels penetrate deeper into the kidney. By E17.5, axons establish connections with nephrons, and this network continues to develop after birth (N'Guetta et al., 2024b). Deletion of peripheral nerves in the kidney does not qualitatively affect the E16.5 endothelial and arterial patterns (Honeycutt et al., 2023). Denervated *Ntrk1* knockout kidneys have, however, fewer glomeruli at birth (N'Guetta, McLarnon, & O'Brien, 2024a). Retrograde tracing has shown that sensory neurons extend from the primary dorsal root ganglia, T10–L2, to the kidney (N'Guetta et al., 2024b). Given the tight innervation of the renal vasculature, especially the renal arteries and arterioles, the sympathetic nerves are optimally positioned to regulate renal blood flow and glomerular filtration rate (McMahon, 2016).

8. Conclusion

Constructing a functional kidney requires the coordinated emergence of collecting ducts, nephrons, vasculature, and nerves, each adhering to specific design principles. The ureteric tree is the first to emerge during development. By virtue of reciprocal signaling with the mesenchyme, branching morphogenesis is coordinated with nephrogenesis. Blood vessels and nerves follow subsequently and can use the branched ureteric tree as a template. The ligand-receptor-based Turing mechanism can explain UB branch point definition in developing lungs and kidneys and is currently the only mechanism that has been shown to be consistent with all the pertinent molecular and genetic data. Interestingly, the largely orthogonal angles between parent and daughter branches in the ureteric tree ensure both the restriction of nephrogenesis to the branch corners (Mederacke et al., 2023) and the restriction of the endpoints of the ureteric tree to a single layer at a uniform distance from the center of the organ (Yu et al., 2019). How the MM defines the branching angles remains an open question. Despite the necessity of mesenchymal GDNF secretion for ureteric branching, nephrogenesis is not responsible for the termination of branching under wildtype conditions (Short et al., 2018). The determinants of kidney size and nephron number thus remain elusive.

While significant progress has been made in understanding the formation of collecting ducts and nephrogenesis, the processes governing the development of the vasculature and the nervous system remain less well understood. Critical questions also persist regarding the establishment of RV polarity, the correct proportional patterning of nephrons despite considerable RV size variations, and the development of fractal architectures in renal trees. Elucidating these design principles and the spectrum of plausible physiological organ architectures holds not only theoretical importance but also practical potential for enhancing disease diagnostics, as deviations from optimal architecture may signal underlying disease states.

Acknowledgments

The authors thank Chengyou Yu for providing Fig. 4, Nikolaos Doumpas for discussions, and acknowledge generous support from SNSF grant 315230_219990.

References

Abler, L. L., Mansour, S. L., & Sun, X. (2009). Conditional gene inactivation reveals roles for Fgf10 and Fgfr2 in establishing a normal pattern of epithelial branching in the mouse lung. *Developmental Dynamics: An Official Publication of the American Association of Anatomists, 238*, 1999–2013.

Adivarahan, S., Menshykau, D., Michos, O., & Iber, D. (2013). *Dynamic image-based modelling of kidney branching morphogenesis*. Berlin, Heidelberg: Springer Berlin Heidelberg106–119.

Akam, M. (1989). Drosophila development: Making stripes inelegantly. *Nature, 341*, 282–283.

Arcuri, P., & Murray, J. D. (1986). Pattern sensitivity to boundary and initial conditions in reaction diffusion-models. *Journal of Mathematical Biology, 24*, 141–165.

Arevalo Perez, J., Gragera Torres, F., Marin Toribio, A., Koren Fernandez, L., Hayoun, C., & Daimiel Naranjo, I. (2013). Angio CT assessment of anatomical variants in renal vasculature: Its importance in the living donor. *Insights Imaging, 4*, 199–211.

Armstrong, N. J., Painter, K. J., & Sherratt, J. A. (2006). A continuum approach to modelling cell-cell adhesion. *Journal of Theoretical Biology, 243*, 98–113.

Bejan, A., Rocha, L., & Lorente, S. (2000). Thermodynamic optimization of geometry: T- and Y-shaped constructs of fluid streams. *International Journal of Thermal Sciences, 39*, 949–960.

Bellusci, S., Grindley, J., Emoto, H., Itoh, N., & Hogan, B. L. (1997). Fibroblast growth factor 10 (FGF10) and branching morphogenesis in the embryonic mouse lung. *Development (Cambridge, England), 124*, 4867–4878.

Bertram, J. F., Douglas-Denton, R. N., Diouf, B., Hughson, M. D., & Hoy, W. E. (2011). Human nephron number: Implications for health and disease. *Pediatric Nephrology (Berlin, Germany), 26*, 1529–1533.

Biot, M. A. (1957). Folding instability of a layered viscoelastic medium under compression. *Proceedings of the Royal Society of London. Series A: Mathematical and Physical Sciences, 242*, 444–454.

Blanc, P., Coste, K., Pouchin, P., Azaïs, J.-M., Blanchon, L., Gallot, D., & Sapin, V. (2012). A role for mesenchyme dynamics in mouse lung branching morphogenesis. *PLoS One, 7*, e41643.

Boucherat, O., Nadeau, V., Berube-Simard, F. A., Charron, J., & Jeannotte, L. (2014). Crucial requirement of ERK/MAPK signaling in respiratory tract development. *Development (Cambridge, England), 141*, 3197–3211.

Bueters, R. R., van de Kar, N. C., & Schreuder, M. F. (2013). Adult renal size is not a suitable marker for nephron numbers: An individual patient data meta-analysis. *Kidney & Blood Pressure Research, 37*, 540–546.

Carrillo, J. A., Murakawa, H., Sato, M., Togashi, H., & Trush, O. (2019). A population dynamics model of cell-cell adhesion incorporating population pressure and density saturation. *Journal of Theoretical Biology, 474*, 14–24.

Carroll, T. J., Park, J. S., Hayashi, S., Majumdar, A., & McMahon, A. P. (2005). Wnt9b plays a central role in the regulation of mesenchymal to epithelial transitions underlying organogenesis of the mammalian urogenital system. *Developmental Cell, 9*, 283–292.

Celliere, G., Menshykau, D., & Iber, D. (2012). Simulations demonstrate a simple network to be sufficient to control branch point selection, smooth muscle and vasculature formation during lung branching morphogenesis. *Biology Open, 1*, 775–788.

Chi, X., Michos, O., Shakya, R., Riccio, P., Enomoto, H., Licht, J. D., ... Costantini, F. (2009). Ret-dependent cell rearrangements in the Wolffian duct epithelium initiate ureteric bud morphogenesis. *Developmental Cell, 17*, 199–209.

Ciruna, B., Jenny, A., Lee, D., Mlodzik, M., & Schier, A. F. (2006). Planar cell polarity signalling couples cell division and morphogenesis during neurulation. *Nature, 439*, 220–224.

Clément, R., Blanc, P., Mauroy, B., Sapin, V., & Douady, S. (2012). Shape self-regulation in early lung morphogenesis. *PLoS One, 7*, e36925.

Combes, A. N., Lefevre, J. G., Wilson, S., Hamilton, N. A., & Little, M. H. (2016). Cap mesenchyme cell swarming during kidney development is influenced by attraction, repulsion, and adhesion to the ureteric tip. *Developmental Biology, 418*, 297–306.

Conrad, L., Runser, S. V. M., Fernando Gomez, H., Lang, C. M., Dumond, M. S., Sapala, A., ... Iber, D. (2021). The biomechanical basis of biased epithelial tube elongation in lung and kidney development. *Development (Cambridge, England), 148*.

Costantini, F., & Kopan, R. (2010). Patterning a complex organ: Branching morphogenesis and nephron segmentation in kidney development. *Developmental Cell, 18*, 698–712.

Counter, W. B., Wang, I. Q., Farncombe, T. H., & Labiris, N. R. (2013). Airway and pulmonary vascular measurements using contrast-enhanced micro-CT in rodents. *American Journal of Physiology. Lung Cellular and Molecular Physiology, 304*, L831–L843.

Daniel, E., Azizoglu, D. B., Ryan, A. R., Walji, T. A., Chaney, C. P., Sutton, G. I., ... Cleaver, O. (2018). Spatiotemporal heterogeneity and patterning of developing renal blood vessels. *Angiogenesis, 21*, 617–634.

Davidson, A. J., Lewis, P., Przepiorski, A., & Sander, V. (2019). Turning mesoderm into kidney. *Seminars in Cell & Developmental Biology, 91*, 86–93.

Davies, J. A., Hohenstein, P., Chang, C. H., & Berry, R. (2014). A self-avoidance mechanism in patterning of the urinary collecting duct tree. *BMC Developmental Biology, 14*.

De Moerlooze, L., Spencer-Dene, B., Revest, J. M., Hajihosseini, M., Rosewell, I., & Dickson, C. (2000). An important role for the IIIb isoform of fibroblast growth factor receptor 2 (FGFR2) in mesenchymal-epithelial signalling during mouse organogenesis. *Development (Cambridge, England), 127*, 483–492.

Deschamps, J., & Duboule, D. (2017). Embryonic timing, axial stem cells, chromatin dynamics, and the Hox clock. *Genes & Development, 31*, 1406–1416.

Dziarmaga, A., Clark, P., Stayner, C., Julien, J. P., Torban, E., Goodyer, P., & Eccles, M. (2003). Ureteric bud apoptosis and renal hypoplasia in transgenic PAX2-Bax fetal mice mimics the renal-coloboma syndrome. *Journal of the American Society of Nephrology: JASN, 14*, 2767–2774.

Eigenbrot, C., & Gerber, N. (1997). X-ray structure of glial cell-derived neurotrophic factor at 1.9 A resolution and implications for receptor binding. *Nature Structural Biology, 4*, 435–438.

Fisher, C. E., Michael, L., Barnett, M. W., & Davies, J. A. (2001). Erk MAP kinase regulates branching morphogenesis in the developing mouse kidney. *Development (Cambridge, England), 128*, 4329–4338.

Francavilla, C., Rigbolt, K. T., Emdal, K. B., Carraro, G., Vernet, E., Bekker-Jensen, D. B., ... Olsen, J. V. (2013). Functional proteomics defines the molecular switch underlying FGF receptor trafficking and cellular outputs. *Molecular Cell, 51*, 707–722.

Fumoto, K., Takigawa-Imamura, H., Sumiyama, K., Kaneiwa, T., & Kikuchi, A. (2017). Modulation of apical constriction by Wnt signaling is required for lung epithelial shape transition. *Development 144, 151-162*.

George, U. Z., & Lubkin, S. R. (2018). Tissue geometry may govern lung branching mode selection. *Journal of Theoretical Biology, 442*, 22–30.

Gierer, A., & Meinhardt, H. (1972). A theory of biological pattern formation. *Kybernetik, 12*, 30–39.

Gill, S. E., Pape, M. C., & Leco, K. J. (2006). Tissue inhibitor of metalloproteinases 3 regulates extracellular matrix–cell signaling during bronchiole branching morphogenesis. *Developmental Biology, 298*, 540–554.

Gill, S. E., Pape, M. C., Khokha, R., Watson, A. J., & Leco, K. J. (2003). A null mutation for Tissue Inhibitor of Metalloproteinases-3 (Timp-3) impairs murine bronchiole branching morphogenesis. *Developmental Biology, 261*, 313–323.

Gleghorn, J. P., Kwak, J., Pavlovich, A. L., & Nelson, C. M. (2012). Inhibitory morphogens and monopodial branching of the embryonic chicken lung. *Developmental Dynamics: An Official Publication of the American Association of Anatomists, 241*, 852–862.

Gomez, H. F., Dumond, M. S., Hodel, L., Vetter, R., & Iber, D. (2021). 3D cell neighbour dynamics in growing pseudostratified epithelia. *eLife, 10*.

Gong, Y., Mo, C., & Fraser, S. E. (2004). Planar cell polarity signalling controls cell division orientation during zebrafish gastrulation. *Nature, 430*, 689–693.

Guo, Y., Chen, T. H., Zeng, X., Warburton, D., Bostrom, K. I., Ho, C. M., ... Garfinkel, A. (2014). Branching patterns emerge in a mathematical model of the dynamics of lung development. *The Journal of Physiology, 592*, 313–324.

Hannezo, E., Scheele, C., Moad, M., Drogo, N., Heer, R., Sampogna, R. V., ... Simons, B. D. (2017). A unifying theory of branching morphogenesis. *Cell, 171*, 242–255.e227.

Hartmann, D., & Miura, T. (2006). Modelling in vitro lung branching morphogenesis during development. *Journal of Theoretical Biology, 242*, 862–872.

Hellmich, H. L., Kos, L., Cho, E. S., Mahon, K. A., & Zimmer, A. (1996). Embryonic expression of glial cell-line derived neurotrophic factor (GDNF) suggests multiple developmental roles in neural differentiation and epithelial-mesenchymal interactions. *Mechanisms of Development, 54*, 95–105.

Hertwig, O. (1884). Das Problem der Befruchtung und der Isotropie des Eies. Eine Theorie der Vererbung. *Jenaische Zeitschrift fur Naturwissenschaft, 18*, 274.

Hess, W. R. (1914). Das Prinzip des kleinsten Kraftverbrauchs im Dienste hämodynamischer Forschung. *Archiv Anat. Physiol. 1*, 62.

Hillen, T., & Painter, K. J. (2009). A user's guide to PDE models for chemotaxis. *Journal of Mathematical Biology, 58*, 183–217.

Hirashima, T., Iwasa, Y., & Morishita, Y. (2009). Dynamic modeling of branching morphogenesis of ureteric bud in early kidney development. *Journal of Theoretical Biology, 259*, 58–66.

Honeycutt, S. E., N'Guetta, P. Y., Hardesty, D. M., Xiong, Y., Cooper, S. L., Stevenson, M. J., & O'Brien, L. L. (2023). Netrin 1 directs vascular patterning and maturity in the developing kidney. *Development (Cambridge, England), 150*.

Horsfield, K., & Cumming, G. (1967). Angles of branching and diameters of branches in the human bronchial tree. *The Bulletin of Mathematical Biophysics, 29*, 245–259.

Horsfield, K., & Cumming, G. (1968). Morphology of the bronchial tree in man. *Journal of Applied Physiology (Bethesda, Md.: 1985), 24*, 373–383.

Hoy, W. E., Hughson, M. D., Bertram, J. F., Douglas-Denton, R., & Amann, K. (2005). Nephron number, hypertension, renal disease, and renal failure. *Journal of the American Society of Nephrology: JASN, 16*, 2557–2564.

Iber, D. (2021). The control of lung branching morphogenesis. *Current Topics in Developmental Biology, 143*, 205–237.

Iber, D., & Mederacke, M. (2022). Tracheal ring formation. *Frontiers in Cell and Developmental Biology, 10*, 900447.

Iber, D., & Menshykau, D. (2013). The control of branching morphogenesis. *Open Biology, 3*, 130088.

Ibrahimi, O. A., Yeh, B. K., Eliseenkova, A. V., Zhang, F., Olsen, S. K., Igarashi, M., ... Mohammadi, M. (2005). Analysis of mutations in fibroblast growth factor (FGF) and a pathogenic mutation in FGF receptor (FGFR) provides direct evidence for the symmetric two-end model for FGFR dimerization. *Molecular and Cellular Biology, 25*, 671–684.

Ihermann-Hella, A., Hirashima, T., Kupari, J., Kurtzeborn, K., Li, H., Kwon, H. N., ... Kuure, S. (2018). Dynamic MAPK/ERK activity sustains nephron progenitors through niche regulation and primes precursors for differentiation. *Stem Cell Reports, 11*, 912–928.

Ihermann-Hella, A., Lume, M., Miinalainen, I. J., Pirttiniemi, A., Gui, Y., Peranen, J., ... Kuure, S. (2014). Mitogen-activated protein kinase (MAPK) pathway regulates branching by remodeling epithelial cell adhesion. *PLoS Genetics, 10*, e1004193.

Kadzik, R. S., Cohen, E. D., Morley, M. P., Stewart, K. M., Lu, M. M., & Morrisey, E. E. (2014). Wnt ligand/Frizzled 2 receptor signaling regulates tube shape and branch-point formation in the lung through control of epithelial cell shape. *Proceedings of the National Academy of Science USA, 111*, 12444–12449.

Keller, G., Zimmer, G., Mall, G., Ritz, E., & Amann, K. (2003). Nephron number in patients with primary hypertension. *The New England Journal of Medicine, 348*, 101–108.

Kim, H. Y., Varner, V. D., & Nelson, C. M. (2013). Apical constriction initiates new bud formation during monopodial branching of the embryonic chicken lung. *Development (Cambridge, England), 140*, 3146–3155.

Kitaoka, H., Takaki, R., & Suki, B. (1999). A three-dimensional model of the human airway tree. *Journal of Applied Physiology (Bethesda, Md.: 1985), 87*, 2207–2217.

Kumaran, G. K., & Hanukoglu, I. (2020). Identification and classification of epithelial cells in nephron segments by actin cytoskeleton patterns. *The FEBS Journal, 287*, 1176–1194.

Kurics, T., Menshykau, D., & Iber, D. (2014). Feedback, receptor clustering, and receptor restriction to single cells yield large Turing spaces for ligand-receptor-based Turing models. *Physical Review. E, Statistical, Nonlinear, and Soft Matter Physics, 90*, 022716.

Lambert, B., MacLean, A. L., Fletcher, A. G., Combes, A. N., Little, M. H., & Byrne, H. M. (2018). Bayesian inference of agent-based models: A tool for studying kidney branching morphogenesis. *Journal of Mathematical Biology, 76*, 1673–1697.

Lang, C., Conrad, L., & Michos, O. (2018). Mathematical approaches of branching morphogenesis. *Frontiers in Genetics, 9*, 673.

Lawlor, K. T., Zappia, L., Lefevre, J., Park, J. S., Hamilton, N. A., Oshlack, A., ... Combes, A. N. (2019). Nephron progenitor commitment is a stochastic process influenced by cell migration. *eLife, 8*.

Lawson, B. A. J., & Flegg, M. B. (2016). A mathematical model for the induction of the mammalian ureteric bud. *Journal of Theoretical Biology, 394*, 43–56.

Lefevre, J., Short, K. M., Lamberton, T. O., Michos, O., Graf, D., Smyth, I. M., & Hamilton, N. A. (2017). Branching morphogenesis in the developing kidney is governed by rules that pattern the ureteric tree. *Development (Cambridge, England)*.

Lin, Y., Zhang, S., Tuukkanen, J., Peltoketo, H., Pihlajaniemi, T., & Vainio, S. (2003). Patterning parameters associated with the branching of the ureteric bud regulated by epithelial-mesenchymal interactions. *The International Journal of Developmental Biology, 47*, 3–13.

Lindstrom, N. O., De Sena Brandine, G., Tran, T., Ransick, A., Suh, G., Guo, J., ... McMahon, A. P. (2018). Progressive recruitment of mesenchymal progenitors reveals a time-dependent process of cell fate acquisition in mouse and human nephrogenesis. *Developmental Cell, 45*, 651–660.e654.

Little, M. H. (2015). Improving our resolution of kidney morphogenesis across time and space. *Current Opinion in Genetics & Development, 32*, 135–143.

Little, M. H., & McMahon, A. P. (2012). Mammalian kidney development: Principles, progress, and projections. *Cold Spring Harb Perspect Biol, 4*.

Lu, B. C., Cebrian, C., Chi, X., Kuure, S., Kuo, R., Bates, C. M., ... Costantini, F. (2009). Etv4 and Etv5 are required downstream of GDNF and Ret for kidney branching morphogenesis. *Nature Genetics, 41*, 1295–1302.

Luo, P. M., Gu, X., Chaney, C., Carroll, T., & Cleaver, O. (2023). Stromal netrin 1 coordinates renal arteriogenesis and mural cell differentiation. *Development (Cambridge, England), 150*.

Mailleux, A. A., Kelly, R., Veltmaat, J. M., De Langhe, S. P., Zaffran, S., Thiery, J. P., & Bellusci, S. (2005). Fgf10 expression identifies parabronchial smooth muscle cell progenitors and is required for their entry into the smooth muscle cell lineage. *Development (Cambridge, England), 132*, 2157–2166.

Majumdar, A., Vainio, S., Kispert, A., McMahon, J., & McMahon, A. P. (2003). Wnt11 and Ret/Gdnf pathways cooperate in regulating ureteric branching during metanephric kidney development. *Development (Cambridge, England), 130*, 3175–3185.

Makarenkova, H. P., Hoffman, M. P., Beenken, A., Eliseenkova, A. V., Meech, R., Tsau, C., ... Mohammadi, M. (2009). Differential interactions of FGFs with heparan sulfate control gradient formation and branching morphogenesis. *Science Signaling, 2*, ra55.

Martin, A. C., & Goldstein, B. (2014). Apical constriction: Themes and variations on a cellular mechanism driving morphogenesis. *Development (Cambridge, England), 141*, 1987–1998.

Mauroy, B., Filoche, M., Weibel, E. R., & Sapoval, B. (2004). An optimal bronchial tree may be dangerous. *Nature, 427*, 633–636.

McMahon, A. P. (2016). Development of the mammalian kidney. *Essays on Developmental Biology, Pt B, 117* 31-+.

Mederacke, M., Conrad, L., Doumpas, N., Vetter, R., & Iber, D. (2023). Geometric effects position renal vesicles during kidney development. *Cell Reports, 42*, 113526.

Meinhardt, H. (1976). Morphogenesis of lines and nets. *Differentiation; Research in Biological Diversity, 6*, 117–123.

Menshykau, D., Blanc, P., Unal, E., Sapin, V., & Iber, D. (2014). An interplay of geometry and signaling enables robust lung branching morphogenesis. *Development (Cambridge, England), 141*, 4526–4536.

Menshykau, D., & Iber, D. (2013). Kidney branching morphogenesis under the control of a ligand-receptor-based Turing mechanism. *Physical Biology, 10*, 046003.

Menshykau, D., Kraemer, C., & Iber, D. (2012). Branch mode selection during early lung development. *PLoS Computational Biology, 8*, e1002377.

Menshykau, D., Michos, O., Lang, C., Conrad, L., McMahon, A. P., & Iber, D. (2019). Image-based modeling of kidney branching morphogenesis reveals GDNF-RET based Turing-type mechanism and pattern-modulating WNT11 feedback. *Nature Communications, 10*, 239.

Metzger, R. J., Klein, O. D., Martin, G. R., & Krasnow, M. A. (2008). The branching programme of mouse lung development. *Nature, 453*, 745–750.

Michos, O., Cebrian, C., Hyink, D., Grieshammer, U., Williams, L., D'Agati, V., ... Costantini, F. (2010). Kidney development in the absence of Gdnf and Spry1 requires Fgf10. *PLoS Genetics, 6*, e1000809.

Michos, O., Goncalves, A., Lopez-Rios, J., Tiecke, E., Naillat, F., Beier, K., ... Zeller, R. (2007). Reduction of BMP4 activity by gremlin 1 enables ureteric bud outgrowth and GDNF/WNT11 feedback signalling during kidney branching morphogenesis. *Development (Cambridge, England), 134*, 2397–2405.

Min, H., Danilenko, D. M., Scully, S. A., Bolon, B., Ring, B. D., Tarpley, J. E., ... Simonet, W. S. (1998). Fgf-10 is required for both limb and lung development and exhibits striking functional similarity to Drosophila branchless. *Genes & Development, 12*, 3156–3161.

Mohamed, T., & Sequeira-Lopez, M. L. S. (2019). Development of the renal vasculature. *Seminars in Cell & Developmental Biology, 91*, 132–146.

Mollard, R., & Dziadek, M. (1998). A correlation between epithelial proliferation rates, basement membrane component localization patterns, and morphogenetic potential in the embryonic mouse lung. *American Journal of Respiratory Cell and Molecular Biology, 19*, 71–82.

Moore, K. A., Huang, S., Kong, Y., Sunday, M. E., & Ingber, D. E. (2002). Control of embryonic lung branching morphogenesis by the Rho activator, cytotoxic necrotizing factor 1. *The Journal of Surgical Research, 104*, 95–100.

Moore, M. W., Klein, R. D., Fariñas, I., Sauer, H., Armanini, M., Phillips, H., ... Rosenthal, A. (1996). Renal and neuronal abnormalities in mice lacking GDNF. *Nature, 382*, 76–79.

Moore, K. A., Polte, T., Huang, S., Shi, B., Alsberg, E., Sunday, M. E., & Ingber, D. E. (2005). Control of basement membrane remodeling and epithelial branching morphogenesis in embryonic lung by Rho and cytoskeletal tension. *Developmental Dynamics: An Official Publication of the American Association of Anatomists, 232*, 268–281.

Mori, H., Gjorevski, N., Inman, J. L., Bissell, M. J., & Nelson, C. M. (2009). Self-organization of engineered epithelial tubules by differential cellular motility. *Proceedings of the National Academy of Sciences USA, 106*, 14890–14895.

Munro, D. A. D., & Davies, J. A. (2018). Vascularizing the kidney in the embryo and organoid: Questioning assumptions about renal vasculogenesis. *Journal of the American Society of Nephrology: JASN, 29*, 1593–1595.

Munro, D. A. D., Hohenstein, P., & Davies, J. A. (2017). Cycles of vascular plexus formation within the nephrogenic zone of the developing mouse kidney. *Scientific Reports, 7*, 3273.

Murray, C. D. (1926a). The physiological principle of minimum work applied to the angle of branching of arteries. *The Journal of General Physiology, 9*, 835–841.

Murray, C. D. (1926b). The physiological principle of minimum work: I. The vascular system and the cost of blood volume. *Proceedings of the National Academy of Sciences USA, 12*, 207–214.

Murray, J., 1993. Mathematical Biology.

Nelson, C. M., VanDuijn, M. M., Inman, J. L., Fletcher, D. A., & Bissell, M. J. (2006). Tissue geometry determines sites of mammary branching morphogenesis in organotypic cultures. *Science (New York, N. Y.), 314*, 298–300.

Nelson, T. R., West, B. J., & Goldberger, A. L. (1990). The fractal lung: Universal and species-related scaling patterns. *Experientia, 46*, 251–254.

N'Guetta, P.-E., McLarnon, S., & O'Brien, L. L. (2024a). Spatiotemporal mapping of renal innervation and impact of in utero fetal denervation on kidney development. *Physiology, 39*.

N'Guetta, P. Y., McLarnon, S. R., Tassou, A., Geron, M., Shirvan, S., Hill, R. Z., ... O'Brien, L. L. (2024b). Comprehensive mapping of sensory and sympathetic innervation of the developing kidney. *Cell Reports, 43*, 114860.

Nogawa, H., & Ito, T. (1995). Branching morphogenesis of embryonic mouse lung epithelium in mesenchyme-free culture. *Development (Cambridge, England), 121*, 1015–1022.

Nordsletten, D. A., Blackett, S., Bentley, M. D., Ritman, E. L., & Smith, N. P. (2006). Structural morphology of renal vasculature. *American Journal of, 291*, H296–H309.

O'Connor, J. P., Hanley, B. M., Mulcahey, T. I., Sheets, E. E., & Shuey, K. W. (2017). N (2) gas egress from patients' airways during LN(2) spray cryotherapy. *Medical Engineering & Physics, 44*, 63–72.

Ohtsuka, N., Urase, K., Momoi, T., & Nogawa, H. (2001). Induction of bud formation of embryonic mouse tracheal epithelium by fibroblast growth factor plus transferrin in mesenchyme-free culture. *Developmental Dynamics: An Official Publication of the American Association of Anatomists, 222*, 263–272.

Oxburgh, L. (2018). Kidney nephron determination. *Annual Review of Cell and Developmental Biology, 34*, 427–450.

Packard, A., Klein, W. H., & Costantini, F. (2021). Ret signaling in ureteric bud epithelial cells controls cell movements, cell clustering and bud formation. *Development (Cambridge, England), 148*.

Paramore, S. V., Trenado-Yuste, C., Sharan, R., Nelson, C. M., & Devenport, D. (2024). Vangl-dependent mesenchymal thinning shapes the distal lung during murine saccula-tion. *Developmental Cell, 59*, 1302–1316.e1305.

Park, W. Y., Miranda, B., Lebeche, D., Hashimoto, G., & Cardoso, W. V. (1998). FGF-10 is a chemotactic factor for distal epithelial buds during lung development. *Developmental Biology, 201*, 125–134.

Parkash, V., Leppanen, V. M., Virtanen, H., Jurvansuu, J. M., Bespalov, M. M., Sidorova, Y. A., ... Goldman, A. (2008). The structure of the glial cell line-derived neurotrophic factor-coreceptor complex: Insights into RET signaling and heparin binding. *The Journal of Biological Chemistry, 283*, 35164–35172.

Pepicelli, C. V., Kispert, A., Rowitch, D. H., & McMahon, A. P. (1997). GDNF induces branching and increased cell proliferation in the ureter of the mouse. *Developmental Biology, 192*, 193–198.

Pepicelli, C. V., Lewis, P. M., & McMahon, A. P. (1998). Sonic hedgehog regulates branching morphogenesis in the mammalian lung. *Current Biology: CB, 8*, 1083–1086.

Perantoni, A. O., Timofeeva, O., Naillat, F., Richman, C., Pajni-Underwood, S., Wilson, C., ... Lewandoski, M. (2005). Inactivation of FGF8 in early mesoderm reveals an essential role in kidney development. *Development (Cambridge, England), 132*, 3859–3871.

Perl, A. J., Schuh, M. P., & Kopan, R. (2022). Regulation of nephron progenitor cell lifespan and nephron endowment. *Nature Reviews. Nephrology, 18*, 683–695.

Peters, K., Werner, S., Liao, X., Wert, S., Whitsett, J., & Williams, L. (1994). Targeted expression of a dominant negative FGF receptor blocks branching morphogenesis and epithelial differentiation of the mouse lung. *The EMBO Journal, 13*, 3296–3301.

Phalen, R. F., Yeh, H. C., Schum, G. M., & Raabe, O. G. (1978). Application of an idealized model to morphometry of the mammalian tracheobronchial tree. *The Anatomical Record, 190*, 167–176.

Pichel, J. G., Shen, L., Sheng, H. Z., Granholm, A. C., Drago, J., Grinberg, A., ... Westphal, H. (1996a). Defects in enteric innervation and kidney development in mice lacking GDNF. *Nature, 382*, 73–76.

Pichel, J. G., Shen, L., Sheng, H. Z., Granholm, A. C., Drago, J., Grinberg, A., ... Westphal, H. (1996b). GDNF is required for kidney development and enteric inner-vation. *Cold Spring Harbor Symposia on Quantitative Biology, 61*, 445–457.

Pleyer, J., & Fleck, C. (2023). Agent-based models in cellular systems. *Frontiers in Physics, 10*.

Prahl, L. S., Viola, J. M., Liu, J., & Hughes, A. J. (2021). The developing kidney actively negotiates geometric packing conflicts to avoid defects. *bioRxiv*.

Qiao, J., Sakurai, H., & Nigam, S. K. (1999). Branching morphogenesis independent of mesenchymal-epithelial contact in the developing kidney. *Proceedings of the National Academy of Sciences of the United States of America, 96*, 7330–7335.

Rahmani, S., Jafree, D. J., Lee, P. D., Tafforeau, P., Jacob, J., Bellier, A., ... Walsh, C. L. (2023). Micro to macro scale analysis of the intact human renal arterial tree with Synchrotron Tomography. *bioRxiv*.

Ramalingam, H., Fessler, A. R., Das, A., Valerius, M. T., Basta, J., Robbins, L., ... Carroll, T. J. (2018). Disparate levels of beta-catenin activity determine nephron progenitor cell fate. *Developmental Biology, 440*, 13–21.

Riccio, P., Cebrian, C., Zong, H., Hippenmeyer, S., & Costantini, F. (2016). Ret and Etv4 promote directed movements of progenitor cells during renal branching morphogenesis. *PLoS Biology, 14*, e1002382.

Rossitti, S., & Lofgren, J. (1993). Optimality principles and flow orderliness at the branching points of cerebral arteries. *Stroke; A Journal of Cerebral Circulation, 24*, 1029–1032.

Runser, S., Vetter, R., & Iber, D. (2024). SimuCell3D: Three-dimensional simulation of tissue mechanics with cell polarization. *Nature Computational Science*.

Rutledge, E. A., Parvez, R. K., Short, K. M., Smyth, I. M., & McMahon, A. P. (2019). Morphogenesis of the kidney and lung requires branch-tip directed activity of the Adamts18 metalloprotease. *Developmental Biology, 454*, 156–169.

Saburi, S., Hester, I., Fischer, E., Pontoglio, M., Eremina, V., Gessler, M., ... McNeill, H. (2008). Loss of Fat4 disrupts PCP signaling and oriented cell division and leads to cystic kidney disease. *Nature Genetics, 40*, 1010–1015.

Sakakura, T., Nishizuka, Y., & Dawe, C. J. (1976). Mesenchyme-dependent morphogenesis and epithelium-specific cytodifferentiation in mouse mammary gland. *Science (New York, N. Y.), 194*, 1439–1441.

Samuel, T., Hoy, W. E., Douglas-Denton, R., Hughson, M. D., & Bertram, J. F. (2007). Applicability of the glomerular size distribution coefficient in assessing human glomerular volume: The Weibel and Gomez method revisited. *Journal of Anatomy, 210*, 578–582.

Sanchez, M. P., Silos-Santiago, I., Frisen, J., He, B., Lira, S. A., & Barbacid, M. (1996). Renal agenesis and the absence of enteric neurons in mice lacking GDNF. *Nature, 382*, 70–73.

Savin, T., Kurpios, N. A., Shyer, A. E., Florescu, P., Liang, H., Mahadevan, L., & Tabin, C. J. (2011). On the growth and form of the gut. *Nature, 476*, 57–62.

Schnakenberg, J. (1979). Simple chemical-reaction systems with limit-cycle behavior. *Journal of Theoretical Biology, 81*, 389–400.

Schuchardt, A., D'Agati, V., Larsson-Blomberg, L., Costantini, F., & Pachnis, V. (1994). Defects in the kidney and enteric nervous system of mice lacking the tyrosine kinase receptor Ret. *Nature, 367*, 380–383.

Sciubba, E. (2016). A critical reassessment of the Hess–Murray law. *Entropy, 18*, 283.

Sekine, K., Ohuchi, H., Fujiwara, M., Yamasaki, M., Yoshizawa, T., Sato, T., ... Kato, S. (1999). Fgf10 is essential for limb and lung formation. *Nature Genetics, 21*, 138–141.

Self, M., Lagutin, O. V., Bowling, B., Hendrix, J., Cai, Y., Dressler, G. R., & Oliver, G. (2006). Six2 is required for suppression of nephrogenesis and progenitor renewal in the developing kidney. *The EMBO Journal, 25*, 5214–5228.

Sequeira Lopez, M. L. S., & Gomez, R. A. (2011). Development of the renal arterioles. *Journal of the American Society of Nephrology, 22*, 2156–2165.

Shakya, R., Jho, E.-H., Kotka, P., Wu, Z., Kholodilov, N., Burke, R., ... Costantini, F. (2005). The role of GDNF in patterning the excretory system. *Developmental Biology, 283*, 70–84.

Sharma, A., Meer, M., Dapkunas, A., Ihermann-Hella, A., Kuure, S., Vainio, S., ... Naillat, F. (2022). FGF8 induces chemokinesis and regulates condensation of mouse nephron progenitor cells. *bioRxiv*.

Short, K. M., Combes, A. N., Lefevre, J., Ju, A. L., Georgas, K. M., Lamberton, T., ... Little, M. H. (2014). Global quantification of tissue dynamics in the developing mouse kidney. *Developmental Cell, 29*, 188–202.

Short, K. M., Combes, A. N., Lisnyak, V., Lefevre, J. G., Jones, L. K., Little, M. H., ... Smyth, I. M. (2018). Branching morphogenesis in the developing kidney is not impacted by nephron formation or integration. *eLife, 7*.

Short, K., Hodson, M., & Smyth, I. (2013). Spatial mapping and quantification of developmental branching morphogenesis. *Development (Cambridge, England), 140*, 471–478.

Sims-Lucas, S., Argyropoulos, C., Kish, K., McHugh, K., Bertram, J. F., Quigley, R., & Bates, C. M. (2009). Three-dimensional imaging reveals ureteric and mesenchymal defects in Fgfr2-mutant kidneys. *Journal of the American Society of Nephrology: JASN, 20*, 2525–2533.

Sobrinho, U., Sampaio, F. J. B., & Favorito, L. A. (2022). Lower pole anatomy of horseshoe kidney and complete ureteral duplication: Anatomic and radiologic study applied to endourology. *International Journal of the Brazilian Society of Urology, 48*, 561–568.

Stopka, A., Kokic, M., & Iber, D. (2019). Cell-based simulations of biased epithelial lung growth. *Physical Biology, 17*, 016006.

Sultan, E., & Boudaoud, A. (2008). The buckling of a swollen thin gel layer bound to a compliant substrate. *Journal of Applied Mechanics, 75*.

Tan, Y., Hu, B., Song, J., Chu, Z., & Wu, W. (2020). Bioinspired multiscale wrinkling patterns on curved substrates: An overview. *Nanomicro Lett, 12*, 101.

Tang, M.-J., Cai, Y., Tsai, S.-J., Wang, Y.-K., & Dressler, G. R. (2002). Ureteric bud outgrowth in response to RET activation is mediated by phosphatidylinositol 3-kinase. *Developmental Biology, 243*, 128–136.

Tang, Z., Hu, Y., Wang, Z., Jiang, K., Zhan, C., Marshall, W. F., & Tang, N. (2018). Mechanical forces program the orientation of cell division during airway tube morphogenesis. *Developmental Cell*.

Tang, N., Marshall, W. F., McMahon, M., Metzger, R. J., & Martin, G. R. (2011). Control of mitotic spindle angle by the RAS-regulated ERK1/2 pathway determines lung tube shape. *Science (New York, N. Y.), 333*, 342–345.

Tang, M. J., Worley, D., Sanicola, M., & Dressler, G. R. (1998). The RET-glial cell-derived neurotrophic factor (GDNF) pathway stimulates migration and chemoattraction of epithelial cells. *The Journal of Cell Biology, 142*, 1337–1345.

Tarnick, J., Elhendawi, M., Holland, I., Chang, Z., & Davies, J. A. (2023). Innervation of the developing kidney in vivo and in vitro. *Biology Open, 12*.

Thurlbeck, A., & Horsfield, K. (1980). Branching angles in the bronchial tree related to order of branching. *Respiration Physiology, 41*, 173–181.

Tikka, P., Mercker, M., Skovorodkin, I., Saarela, U., Vainio, S., Ronkainen, V. P., ... Schaefer, F. (2022). Computational modelling of nephron progenitor cell movement and aggregation during kidney organogenesis. *Mathematical Biosciences, 344*, 108759.

Treanor, J. J., Goodman, L., de Sauvage, F., Stone, D. M., Poulsen, K. T., Beck, C. D., ... Rosenthal, A. (1996). Characterization of a multicomponent receptor for GDNF. *Nature, 382*, 80–83.

Turing, A. M. (1952). The chemical basis of morphogenesis. *Philosophical Transactions of the Royal Society B, 237*, 37–72.

Uylings, H. (1977). Optimization of diameters and bifurcation angles in lung and vascular tree structures. *Bulletin of Mathematical Biology, 39*, 509–520.

Varner, V. D., Gleghorn, J. P., Miller, E., Radisky, D. C., & Nelson, C. M. (2015). Mechanically patterning the embryonic airway epithelium. *Proceedings of the National Academy of Science USA, 112*, 9230–9235.

Vetter, R. (2015). Interaction and packing of thin objects. *ETH Zurich*.

Volckaert, T., Campbell, A., Dill, E., Li, C., Minoo, P., & De Langhe, S. (2013). Localized Fgf10 expression is not required for lung branching morphogenesis but prevents differentiation of epithelial progenitors. *Development (Cambridge, England), 140*, 3731–3742.

Warburton, D., Bellusci, S., Del Moral, P. M., Kaartinen, V., Lee, M., Tefft, D., & Shi, W. (2003). Growth factor signaling in lung morphogenetic centers: Automaticity, stereotypy and symmetry. *Respiratory Research, 4*, 5.

Watanabe, M., & Kondo, S. (2015). Is pigment patterning in fish skin determined by the Turing mechanism? *Trends in Genetics: TIG, 31*, 88–96.

Weibel, E. R. (1963). *Morphometry of the human lung*. Heidelberg: Springer Berlin.

Weibel, E. R., & Gomez, D. M. (1962). Architecture of the human lung. Use of quantitative methods establishes fundamental relations between size and number of lung structures. *Science (New York, N. Y.), 137*, 577–585.

Wellik, D. M., Hawkes, P. J., & Capecchi, M. R. (2002). Hox11 paralogous genes are essential for metanephric kidney induction. *Genes & Development, 16*, 1423–1432.

White, A. C., Lavine, K. J., & Ornitz, D. M. (2007). FGF9 and SHH regulate mesenchymal Vegfa expression and development of the pulmonary capillary network. *Development (Cambridge, England), 134*, 3743–3752.

Williams, D., Kenyon, A., & Adamson, D. (2010). Chapter ten - Physiology. In P. Bennett, & C. Williamson (Eds.). *Basic science in obstetrics and gynaecology (fourth edition)* (pp. 173–230). Churchill Livingstone.

Wilson, T. A. (1967). Design of the bronchial tree. *Nature, 213*, 668–669.

Xu, H., Sun, M., & Zhao, X. (2017). Turing mechanism underlying a branching model for lung morphogenesis. *PLoS One, 12*, e0174946.

Yu, W., Marshall, W. F., Metzger, R. J., Brakeman, P. R., Morsut, L., Lim, W., & Mostov, K. E. (2019). Simple Rules Determine Distinct Patterns of Branching Morphogenesis. *Cell systems, 9*, 221–227.

Zamir, M. (1977). Shear forces and blood vessel radii in the cardiovascular system. *The Journal of General Physiology, 69*, 449–461.

Zeng, H., Ali, S., Sebastian, A., Ramos-Medero, A. S., Albert, I., Dean, C., & Liu, A. (2024). CPLANE protein INTU regulates growth and patterning of the mouse lungs through cilia-dependent Hh signaling. *Developmental Biology*.

Zhang, Z., Quinlan, J., Hoy, W., Hughson, M. D., Lemire, M., Hudson, T., ... Goodyer, P. (2008). A common RET variant is associated with reduced newborn kidney size and function. *Journal of the American Society of Nephrology: JASN, 19*, 2027–2034.

Zhao, Y., Cao, Y., Feng, X.-Q., & Ma, K. (2014). Axial compression-induced wrinkles on a core–shell soft cylinder: Theoretical analysis, simulations and experiments. *Journal of the Mechanics and Physics of Solids, 73*, 212–227.

Zhu, X., & Yang, H. (2018). Turing instability-driven biofabrication of branching tissue structures: A dynamic simulation and analysis based on the reaction(-)diffusion mechanism (dagger). *Micromachines (Basel), 9*.

Zubkov, V. S., Combes, A. N., Short, K. M., Lefevre, J., Hamilton, N. A., Smyth, I. M., ... Byrne, H. M. (2015). A spatially-averaged mathematical model of kidney branching morphogenesis. *Journal of Theoretical Biology, 379*, 24–37.